**Paper:**
Paul, F., Bolch, T., Kääb, A., Nagler, T., Nuth, C., Scharrer, K., Shepherd, A., Strozzi, T., Ticconi, F., Bhambri, R., Berthier, E., Bevan, S., Gourmelen, N., Heid, T., Jeong, S., Kunz, M., Lauknes, T., Luckman, A., Merryman Boncori, J., Moholdt, G., Muir, A., Neelmeijer, J., Rankl, M., VanLooy, J. & Van Niel, T. (2015). The glaciers climate change initiative: Methods for creating glacier area, elevation change and velocity products. *Remote Sensing of Environment, 162*, 408-426.
http://dx.doi.org/10.1016/j.rse.2013.07.043

# The Glaciers Climate Change Initiative: Algorithms for creating glacier area, elevation change and velocity products

Frank Paul[1], Tobias Bolch[1], Andreas Kääb[2], Thomas Nagler[3], Christopher Nuth[2], Killian Scharrer[3], Andrew Shepherd[4], Tazio Strozzi[5], Francesca Ticconi[4], Rakesh Bhambri[6], Etienne Berthier[7], Suzanne Bevan[8], Matthias Braun[9], Noel Gourmelen[10], Torborg Heid[2], Seongsu Jeong[11], Matthias Kunz[12], Tom Rune Lauknes[13], Adrian Luckman[14], John Merryman[15], Geir Moholdt[16], Alan Muir[17], Julia Neelmeijer[18], Jeffrey VanLooy[19], Thomas Van Niel[20]

1 Department of Geography, University of Zurich, Switzerland, frank.paul@geo.uzh.ch
2 Department of Geosciences, University of Oslo, Norway
3 Environmental Earth Observation IT GmbH (ENVEO), Innsbruck, Austria
4 School of Earth and Environment, University of Leeds, United Kingdom
5 Gamma Remote Sensing AG, Gümligen, Switzerland
6 Centre for Glaciology, Wadia Institute of Himalayan Geology
7 CNRS, Universitè de Toulouse, LEGOS, 14 avenue Ed. Belin, Toulouse 31400, France
8 Swansea University, Swansea, Uk
9 University of Erlangen, Erlangen, Germany
10 Noel Gourmelen, University Strasbourg, Strasbourg, France
11 Ohio State University, Columbus (OH), USA
12 School of Civil Engineering and Geosciences, Cassie Building, Newcastle University, NE1 7RU, UK
13 NORUT, Oslo, Norway
14 Swansea University, Swansea, SA2 8PP, Wales, UK
15 Danish Technical University (DTU), Copenhagen, Denmark
16 Centre for Polar Observation and Modelling, United Kingdom
17 Scripps Institution of Oceanography, La Jolla, California
18 Geoforschungszentrum Potsdam (GFZ), Potsdam, Germany
19 Department of Earth System Science and Policy, University of North Dakota, Grand Forks, ND, 58202, USA
20 CSIRO Land and Water, Private Bag No. 5, Wembley, WA 6913, Australia

## Abstract

Glaciers and their changes are increasingly monitored from a wide range of satellite sensors. Due to the often remote location of glaciers in inaccessible and high-mountain terrain, satellite observations complement ground-based measurements very well. Furthermore, satellite data provide observations of glacier characteristics that are difficult to monitor from ground. In the Glaciers_cci project three of these well-observable characteristics are investigated in detail: glacier area, elevation changes (ELC) and surface velocity (VEL). We use optical sensors to automatically derive area, digital elevation models from two points in time and repeat altimetry for ELC, and optical and microwave imaging sensors for VEL. For the latter, the two sensor types again provide complimentary information in regard to their spatio-temporal coverage. While some products can be generated largely automatically (ELC from altimetry and VEL), the others require interaction by the analyst. Largely based on round robin experiments for each of the products, we suggest in this contribution the most suitable algorithms for product creation and describe them here along with remarks on their practical implementation. In many cases the details on the latter are even more important for creation of high-quality products than the basic algorithm itself.

# 1. Introduction

Glaciers are considered key indicators of climate change due to their sensitive reaction to even small climatic changes (e.g. Lemke et al., 2007). This is basically a result of the ice being at the pressure melting point (under terrestrial conditions and for temperate glaciers), i.e. each surplus of energy is converted to melt the ice. Glaciers adjust their extent to be in balance with the prevailing climatic conditions that largely control mass gain and loss. The balancing force is glacier flow that transports mass from the accumulation to the ablation regions. The determination of glacier changes that occur as a reaction to a change in climate thus involves the measurement of changes in glacier surface elevation, flow velocity and size/length, among others (e.g. snow covered area at the end of the melting period). Variations in these parameters are related to each other, but at varying time scales. For example, the annual mass budget is a direct reaction to the prevailing meteorological conditions over a year, whereas changes in flow velocity result from a more long-term change in the nourishment of a glacier. Also changes in glacier size follow more long-term climatic changes, in which a direct cause and effect relation is difficult to resolve.

Due to the often remote location of glaciers and the large areas covered by them, satellite-based measurements of glacier changes complement field-based surveys in an ideal way. They can largely extend the number of glaciers measured, the time period covered and the parameters that can be assessed. The wide range of available sensors (e.g. imaging sensors and altimeters working in both the optical and microwave region of the electromagnetic spectrum) and archives from ongoing and historic missions combined with already existing geospatial information like digital elevation models (DEMs) or former glacier outlines (e.g. available through the GLIMS initiative, www.glims.org), allows measurement of a wide range of glaciologically relevant parameters (Kargel et al., 2005; Malenovsky et al., 2012). The Glaciers_cci project focuses on three of them: glacier area, elevation changes (from DEMs and altimetry), and velocity fields (from optical and microwave sensors). Numerous algorithms are available for product retrieval from each of the input data sets and sensor combinations (see 2.1). They differ in complexity (from simple band math operations such as division / subtraction of raw data to rather complex calculations and processing lines) and the required operator interaction (e.g. manual control and editing to almost fully automatic). However, a pre-, main and post processing stage is common and some of these stages can be largely automated allowing more or less operational (e.g. script based) data processing.

In the Glaciers_cci project, the various algorithms along with their specific post-processing / editing operations were investigated in four round robin experiments (one for area and velocity, two for elevation change) to find the most suitable algorithms for data processing and improved error characterization of the generated products. In this contribution, a short overview is provided on algorithms applied for generating the three products and the final algorithm selection is presented in more detail. For the more simple algorithms, we also describe the lessons learned from the round robin, as well as the challenges and main pitfalls during the pre- and post-processing stages by human operators, as they involve some degree of subjectivity and largely govern the quality of the final product. Our study regions cover different mountain ranges around the globe (Fig. 1).

*Figure 1*

# 2. Glacier area

## 2.1 Background and previous works

Satellite data have been used to study glaciers from the very beginning of their availability. Starting with the mapping of different ice and snow facies using the 80 m resolution Landsat Multi Spectral Scanner (MSS) sensor in the 1970s (Østrem, 1975; Rott, 1976) and the 30 m Landsat Thematic Mapper (TM) sensor a decade later (e.g. Hall et al., 1987; Williams et al., 1991), the 1990s saw mapping of glacier extent and first studies on change assessment with TM data (e.g. Bayr et al., 1994, Aniya et al., 1996, Jacobs et al. 1997). A wide range of methods were applied in these studies to map glacier extents. They range from full manual on-screen digitization (e.g. Rott and Markl, 1989; Williams et al., 1997), to the segmentation of ratio images (e.g. Bayr, 1994; Rott, 1994; Paul, 2002) and various supervised (Maximum-Likelihood) and unsupervised (ISODATA clustering) algorithms (e.g. Aniya et al., 1996; Sidjak and Wheate, 1999). They all utilize the very low spectral reflectance of ice and snow in the shortwave infrared (SWIR) versus the high reflectance in the visible spectrum (VIS) to identify glaciers (e.g. Dozier, 1989). These methods were compared in regard to their performance (accuracy, time taken) in a relative sense (e.g. Albert, 2002; Paul and Kääb, 2005), but also compared to higher resolution datasets to determine their absolute accuracy (e.g. Paul et al., 2003; Andreassen et al., 2008). In the last decade Landsat TM data were used more systematically to create glacier inventories in many regions of the world (e.g. Bolch et al. 2010; Frey et al., 2012; Le Bris et al. 2011; Paul et al., 2011; Racoviteanu et al., 2008; Shangguan et al., 2009). Several of these studies were only possible thanks to the opening of the Landsat archive at USGS and the provision of already orthorectified images (Level 1T product) in the common GeoTif format (Wulder et al., 2012).

Converting the glacier outlines to inventory information involves digital intersection with drainage divides and calculation of topographic parameters (e.g. minimum, mean, and maximum elevation) for each glacier entity. Practical guidelines (e.g. Raup and Kahlsa, 2007; Racoviteanu et al., 2009) and general advice (e.g. Paul et al., 2002 and 2009) was made available to the analysts to guarantee a consistent data processing. The majority of the generated outlines are stored as shapefiles (a vector format) along with their meta-information in the GLIMS (Global Land Ice Measurements from Space) glacier database for free access by the community (Raup et al., 2007). In the meantime, one globally complete dataset has been made available as the Randolph Glacier Inventory (RGI) via the GLIMS website (Arendt et al., 2012).

## 2.1 Pre-processing

The first step in creating accurate glacier outlines from satellite data is the selection of suitable images. This is a non-trivial task, as snow and cloud conditions are often not optimal (e.g. clouds covering parts of an otherwise perfect scene) and it might be required to combine outlines from more than one scene of the same region (e.g. Bolch et al., 2010; Le Bris et al., 2011; Frey et al., 2012; Rastner et al., 2012; Bajracharya and Mool, 2011). Experience from the past decade has shown that it is not advisable to use scenes with adverse snow conditions (i.e. seasonal snow is found outside of glaciers) for glacier mapping. The workload to correct these regions afterwards can be enormous as a decision on thousands of small polygons has to be made. A size-filter is an option to remove many of the smallest snow patches, but if they are as large as glaciers (e.g. >0.05 $km^2$), manual editing might have to be applied. As the workload can be very high for this editing and the quality of the result still unsatisfactory, it is strongly recommended to use only the best available scenes (in regard to snow conditions) for glacier

mapping. Really beneficial today is the fast availability of full resolution scene quicklooks (<10 MB) from the glovis.usgs.gov website that allows a quick analysis of the snow and cloud conditions before download and processing of the original data.

Once scenes are selected, they have to be downloaded, converted to the format of the digital image processing software used, and analysed in more detail. For this purpose and the later manual editing, we recommend to generate contrast enhanced false-colour composites using the TM equivalent bands 3, 2, 1; 4, 3, 2; and 5, 4, 3 as RGB, respectively. The latter is important for proper identification of glaciers (blue-green) and clouds (white), while the first helps to identify ice and snow in shadow during visual inspection. The typical false colour infrared image (bands 432) is useful for the identification of water surfaces that show a wide range of colours in this band combination. As the main processing works on the raw digital numbers, the otherwise often required atmospheric and/or topographic correction of the scenes must not be applied.

**2.2. Main processing (Classification of glaciers)**

Glacier ice originates from metamorphosed and compressed snow resulting in spectral characteristics that are similar to those of snow with large grain size (Hall et al., 1987). At the end of the ablation period (when snow cover is minimal) and from a remote sensing perspective, the glacier surface is composed of bare ice, snow, dirt / debris / rocks and liquid water; all under highly variable illumination conditions (e.g. located in direct sunlight or cast shadow). Heavily crevassed areas can also lack spectral contrast and debris-covered glacier parts are spectrally very similar to the surrounding terrain. On the other hand, dirt often covers the bare ice on a micro scale, hence providing a sufficiently large portion of ice being visible in a 30 by 30 m resolution satellite image and thus allows its identification. Apart from the well-established band ratio methods (see below), several other methods were applied to classify glaciers (see 2.1). Most of them (e.g. band ratio, NDSI, ISODATA clustering, principal component analysis, decision tree classifiers) were also applied by the participants of the round robin on glacier area, which is largely described in Paul et al. (in press) as its focus was on accuracy assessment. However, for one challenging test site in the Himalaya (with many devris covered glaciers) the round robin participants had to create glacier outlines from their algorithm of choice. For a subregion of the test site they were asked to correct wrongly classified outlines manually using only spectral information for identification (i.e. a DEM was not provided). An overlay of all resulting glacier outlines reveals differences only at the level of individual pixels for clean ice (Fig. 2), but large differences in debris-covered regions (e.g. not recognized it at all) where manual corrections are required. With these results in mind, we describe in the following only the more simple methods with little analyst interaction.

*Figure 2*

As shown previously (e.g. Albert 2002; Paul et al., 2002; Paul and Kääb, 2005), the 'best' method in this regard (fast, simple, accurate, robust) is the calculation of a simple band ratio with the TM equivalent bands 3 (red) and 5 (SWIR) and an additional threshold in TM1 (for improved mapping in shadow) using the raw digital numbers. When TM4/TM5 is applied instead, the TM1 threshold is not required as TM4 is much less sensitive to atmospheric scattering than TM3. The TM3/TM5 ratio also tends to map all water surfaces as glaciers (depending on turbidity), which is not the case with TM4/TM5. On the other hand, TM4/TM5 tends to miss regions with ice and snow in deep cast shadow (e.g. Andreassen et al., 2008) but maps vegetation in shadow. Hence, preference for one or the other band combination depends

on the water / vegetation conditions in the respective regions. Also the normalized difference snow index (NDSI) computed as (TM2 + TM5) / (TM2 - TM5) is applied widely for glacier mapping (e.g. Racovitenau et al., 2008; Gjermundsson et al., 2011), but it requires more user interaction as the atmospheric scattering in TM2 (green) is high and this so-called path radiance has to be subtracted beforehand (Paul and Kääb, 2005). This requires calculation of a histogram, determination of its lowest suitable value, and subtraction of this value from the original band before the NDSI can be applied.

To get a binary (black and white) glacier map out of the (floating point) band ratio, a threshold must be applied. Typical values published so far are in the 2.0 +/-0.5 range for the ratio and 50 +/-20 for the TM1 correction, partly depending on the band combination used and the local atmospheric conditions. For other sensors (ASTER, SPOT) slightly different values have to be selected. As shown in Fig. 3a, the threshold for the ratio is rather robust, i.e. only a few pixels change when 1.8, 1.9 or 2.0 is used as a threshold (cf. Paul and Hendriks, 2010). However, the TM1 threshold is more sensitive and small changes in the threshold value (e.g. +/-10) can make a large difference in the mapped glacier region (Fig. 4). The general advice for threshold selection is thus to use a value that minimizes the workload for post-processing (i.e. corrections required in shadow regions). The correct values are found by first selecting the threshold for the band ratio and then optimizing the TM1 value (for ASTER and SPOT sensors the green bands work as well). When comparing glacier outlines from different thresholds, the correct value is where most ice is mapped (i.e. towards low threshold values) but the noise level remains low. As can be seen in Fig. 4, more and more ice and snow in shadow is mapped towards the lower thresholds, but the lowest value (60) starts to introduce noise (small yellow dots). In this case 65 was finally selected as a threshold for TM1. After the binary image is created, a spatial filter (e.g. 3 by 3 median) may be applied without changing the glacier area much (cf. Paul and Hendriks, 2010), i.e. the number of removed and added pisels is about similar as can be ssen in Fig. 3b. In this regard it is acceptable to have some noisy pixels left in the previous step, as they will be removed by the filter. Once the final binary glacier map is created, a raster-vector conversion is applied for the subsequent editing of polygons in the vector domain.

*Figure 3*

In regard to a potential automated detection of the correct threshold, it remains to be tested whether the use of at-satellite planetary reflectance (correcting for solar elevation and sun-earth distance) would result in more unique threshold values globally. While it is appealing to derive automated glacier area cover estimation in an operational batch processing at space agencies, it will not overcome the detailed manual analysis needed to create the most accurate product required by the community. One example is that atmospheric conditions are too variable (also within a scene) to work with a fixed threshold value only. For example, locally variable atmospheric conditions (e.g. due to fog, haze or optically thin clouds) might require to use two different thresholds within one scene or even to map the upper and lower parts of glaciers from two different scenes (Le Bris et al., 2011) and combine both datasets afterwards.

*Figure 4*

**2.3 Post-processing (Manual editing)**

The post-processing may be divided into three steps, (i) the correction of the outlines, (ii) the digital intersection with drainage divides, and (iii) the calculation of topographic parameters.

The latter has already been described in detail by Paul et al. (2009) and (ii) was already suggested in Paul et al. (2002). The generation of drainage divides for glaciers from watershed analysis is, among others, described by Bolch et al. (2010) or Manley (2008). We will thus focus on the first point (i), the manual editing. For practical reasons it is advisable to first remove quickly all gross errors. Misclassified water surfaces not in contact with glacier ice or those with ice bergs or sea ice on it tend to create thousands of polygons that reduce processing speed. These can be easily selected in the vector domain and deleted. The more detailed work is then correction of debris-covered parts, shadow regions, local clouds hiding a glaciers perimeter and terminus digitizing of glaciers calving into lakes or the sea. In this step the various false-colour composites created during the pre-processing are useful for correcting the outlines, but simple layer-stacking of three bands in the software used might also work for proper identification. High-resolution images (e.g. Ikonos, Quickbird or aerial) or those that are sometimes available in Google Maps™ or similar tools can be used to aid in the correct interpretation. In cases where the exact boundary is unclear (e.g. due to deep shadow or clouds), we suggest to use this additional information and, if a DEM is available, to also create a shaded relief and digitize the outline as a best-guess interpretation. If all this is not available, it is possible to identify such highly uncertain sections of the glacier perimeter by digitizing straight lines. This facilitates later correction and can also be used to assign a higher uncertainty to such a segment in the GLIMS database. Of course, when additional information is available (e.g. a DEM) a more educated guess of the outline can be digitized. For a discussion of the other more methodological challenges in identifying which parts of a glacier need to be included (e.g. attached perennial snow patches) we refer to Racoviteanu et al. (2009).

## 3. Glacier elevation changes from DEM differencing

### 3.1 Background

Measuring glacier elevation changes is a commonly applied method for estimating volume and mass changes of glaciers at local and regional scales. The so-called geodetic method has been applied for decades to DEMs derived from aerial photographs (Finsterwalder, 1954) and, for the last decade, to DEMs derived from space-borne data. For individual glaciers, geodetic mass balances over decadal periods are useful to check the consistency with cumulated *in-situ* measured mass balance and to determine whether bias has accumulated in the *in-situ* measurements (e.g. Cox and March, 2004; Zemp et al., 2010). Importantly, the same method allows determination of region wide mass balance due to the large spatial coverage of recent space-borne DEMs (e.g. Berthier et al., 2010; Bolch et al., 2011; Gardelle et al., 2012b; Larsen et al., 2007; Paul and Haeberli, 2008; Schiefer et al., 2007; Willis et al., 2012). The one critical assumption required for converting elevation and volume changes into mass changes is the density of the material gained or lossed (cf. Kääb et al., 2012).

The variation in techniques available to derive DEMs limit fully automated results without manual inspection. DEMs may be generated through airborne or spaceborne photogrammetry using optical or microwave images, RADAR interferometry, and LIDAR scanning. Each of these methods have different types of errors (in glacier settings) that must be considered independently. For example, photogrammetry is dependent upon good visual contrast in the images, while radar interferometry may provide elevations of a layer below the glacier surface, and LIDAR have range biases or waveform saturation problems (Fricker et al., 2005; Joerg et. al., 2012). It is important to note that the impact of these and other general method

characteristics will vary considerably depending on glacier type and setting, and on specific ground conditions during acquisition, so that DEM quality is highly variable in space, time and with the method employed. Table 3.1 provides an overview of automatically generated DEMs available for computing glacier elevation changes globally.

Glaciers_CCI focuses on the sole extraction of glacier elevation changes as the conversion to mass changes can then be completed by the users with their preferred density assumption. Subtraction of two matrices (i.e. DEMs) is trivial when having the same ground resolution; however ensuring the DEMs are properly aligned, that their resolutions are similar, and the detection of other higher-order biases remains difficult. At this stage of development, co-registration algorithms for determining mis-alignments between the multitemporal DEMs were tested. The general procedures used for deriving glacier elevation changes from multitemporal DEMs are outlined below. The slave DEM was defined as that which was co-registered to the master DEM.

- *Pre-Processing*: Ensure both DEMs contain the same datum and projection and apply transformations if required. Selection of suitable terrain for input into the DEM co-registration routine, defined as stable and unchanging, i.e. outside glaciers (requires input from the glacier area product), no water bodies, no clouds or data voids and assuming limited vegetation effects or removing them. This portion of the DEM is analyzed to determine the co-registration parameters and later for validation of products and accuracy quantification. The last part of the pre-processing procedures involve the co-registeration of the slave DEM to master DEM.
- *Main-Processing*: Resample one DEM to the other such that their grids are consistent and subtract the oldest DEM from the newest DEM to estimate elevation differences.
- *Post-Processing*: A major part of the post-processing is to manually / (semi) automatically check for various other biases, e.g. from rotations, along/cross track sampling issues, satellite jitter, and scale problems. Use the selected stable terrain for random and systematic uncertainty estimation. Histogram adjustments may be required. Other post processing procedures include filtering or downsampling (by averaging) the glacier elevation changes to reduce noise effects.

### 3.2 Pre-processing

To compute elevation differences, the DEMs must be in the same projection. Commonly, rectangular coordinate systems such as the Universal Transverse Mercator (UTM) system are used as this projection preserves distances and areas and re-projection algorithms are commonly available in GIS software. Multi-temporal DEMs may also have different spatial resolutions which requires a resampling of one or both of the DEMs to make them congruent. Resampling must be performed using algorithms more advanced than nearest neighbor (i.e. bilinear, bi-cubic, etc), as nearest neighbor techniques incorporate sub-pixel horizontal misalignments between the data. The simplest method to determine whether the two DEMs are co-registered is to map their differences in gray-scale with an equal color ramp centered around 0 (Nuth and Kääb, 2011). If the grayscale differences resemble the terrain (i.e. looks like a DEM hillshade) then there is a horizontal misalignment. The bearing of the overall shift between DEMs is associated with the aspect having the highest positive bias, whereas the magnitude of the bias is associated with the slope of the site (Van Niel et al., 2008), see Figure 3.1. The relationship between elevation difference and both slope and aspect were formally defined in (Nuth and Kääb, 2011), summarised below.

*The round robin experiment*

The round robin for deriving glacier elevation changes from DEM differencing tested co-registration algorithms. The experiment covered the Southern Alps of New Zealand using two ASTER DEMs (2002 and 2006) and the SRTM (2000), with optional auxiliary ICESat data. A common glacier mask (Gjermundsen et al., 2011) was provided together with the elevation datasets. Participants were asked to co-register the three DEMs to each other, and if possible, also to ICESat, return their co-registration parameters ($\Delta x$, $\Delta y$, $\Delta z$) and an elevation change grid (2006-2000). Six contributions implemented in various software products or combinations thereof (IDL, Matlab, ArcGIS, ENVI, PCI Geomatica, GMT tools, GDAL) were received. Three automatic algorithms were tested: (A) a robust surface matching technique solving for the linear translation, rotation and scale (Gruen and Akca, 2005; Miller et al., 2009; Miller et al., 2008), (B) an iterative minimization of the elevation difference residuals (Berthier et al., 2007; Rodriguez et al., 2006), (C) an analytical solution for translation only based upon terrain slope and aspect (Kääb, 2005a; Nuth and Kääb, 2011) and (D) one semi-manual approach based upon terrain slope (VanLooy and Foster, 2008). The first algorithm minimizes the Euclidean distance between two surfaces while the other algorithms rely on the minimization of elevation difference residuals over assumed stable terrain. The strategy for analyzing the results was to visualize the elevation change grids in grayscale to determine whether some misalignment remained ("false hillshade") and to triangulate (vector sum) three or more co-registration vectors between the datasets to test internal consistency. Theoretically, the vector sums should be 0 for the horizontal and vertical components, but in practice residuals are present reflecting the method's uncertainty.

Table 3.2 shows the co-registration vectors and triangulation between the SRTM DEM (2000) and two ASTER DEMs (2002, 2006) for three contributions of the three automatic algorithms tested. The specific co-registration parameters are similar for methods A and C (Table 3.2), but different for Method B when the SRTM DEM is involved. The reason behind this variation is that the SRTM DEM was provided with an additional tif world file for geocoding which does not specify the pixel definition of centre or corner. Nonetheless, the triangulation of co-registration parameters for all three algorithms resulted in similar sub-pixel residuals despite the variation in co-registration parameters. The "false-hillshade" of the DEM differences for 4 out of 6 contributions displayed only small hints of the terrain suggesting that the co-registration was successful and misalignment properly removed. In two cases, the terrain was clearly visible despite proper triangulation residuals. This occurred after co-registration in one software, and final differencing in a different software, specifically from a nearest neighbor resampling that is default within the *Raster Calculator Tool* of the ESRI ArcGIS software. In some of the contributions using the same algorithms (not shown here), the triangulated residuals resulted in magnitudes of similar order to the pixel and half pixel sizes of the DEMs. We attribute this artifact also to the definition of the pixel corner vs. center in the various softwares, and results specifically when switching softwares within a single processing chain. In summary, one of the major lessons learned from this round robin is that any automated DEM differencing processing chain should be maintained within one software product to avoid propagation of pixel definition problems.

*Algorithm selection*

All three automatic algorithms result in similar sub-pixel accuracies when co-registering DEMs. When co-registering a DEM to ICESat, the analytical solution using slope/aspect out-performed the other methods (Table 3.2). In terms of computational efficiency, the implementation of the analytical solution (C) require 2-3 iterations whereas both the robust

surface matching (A) and the image matching (B) require exponentially more iterations. For development within Glaciers_cci, the analytical co-registration algorithm is chosen due to the robustness to operate with various input datasets (i.e. the algorithm works equally using one DEM and one vector data set such as ICESat as between two DEMs) as well as algorithm efficiency. The algorithm is well described (Nuth and Kääb, 2011), and is based upon minimizing the residuals between the left and right sides of the following equation using the population of elevation differences on the stable terrain (*dh*):

$$\frac{dh}{\tan(\alpha)} = a \cdot \cos(b - \psi) + c$$

where $\alpha$ is the terrain slope, $\psi$ is the terrain aspect, and the parameters $a$ and $b$ are the magnitude and direction, respectively, of the co-registration vector and $c$ is the mean bias between the DEMs divided by the mean slope of the selected terrain. The implementation for minimization is not strictly defined, and we use a robust linear least squares method (implemented in Matlab) to determine unknown *a, b* and *c*. Since the solution to this analytical relationship is solved using a non-analytical surface (i.e. the terrain), the first solution may not be the final solution and iteration of the process is required to arrive at an ultimate solution. Typically 1-2 iterations are required (depending upon the minimization routine); we stop the process when improvement of the standard deviation is less than 2%. An example of the co-registration procedure using the selected algorithm can be seen in Figure 5.

### 3.2 Main Processing

After determining the co-registration parameters, the original slave DEM is translated by adjusting the corner coordinates by the horizontal co-registration parameters ($\Delta x$, $\Delta y$) and the mean bias ($\Delta z$) is removed/subtracted. Therefore, no resampling of the original pixels is required in this adjustment. Resampling of one of the DEMs is then required to unify the two DEM pixel sizes and locations. In many cases (and in our round robin experiment), the coarser resolution DEM is up-sampled to the finer resolution DEM. However, this introduces data at a scale that is not measured by the technique, possibly introducing artifacts (Gardelle et al., 2012a; Paul, 2008). We suggest to down-sample the DEM with the finer resolution to that of the coarser resolution, preferably using block averaging filters if one DEM pixel size is at least two times larger than the other DEM pixel. After the DEMs spatially cohere to each other (in space and resolution), a matrix (map) of glacier elevation changes is generated by subtracting the two co-registered matrices (DEMs).

### 3.3 Post-processing

The co-registration procedure is an initial step within the generation of the glacier elevation changes from DEM differencing. A number of other artifacts (biases) have been encountered in DEM differencing including C-Band penetration into snow-ice of the SRTM DEM (Berthier et al., 2006; Gardelle et al., 2012a; Kääb et al., 2012), along-track satellite attitude pointing biases in ASTER DEMs (Nuth and Kääb, 2011) and many other potential corrections such as sensor specific influences (e.g. Berthier et al., 2007; Paul, 2008; Bolch, 2008) and/or rotation/scale distortions may need to be considered. However, it remains open what exactly could cause and what the physical meaning behind potential rotational/scale effects in differenced DEMs could be and whether their correction is significant. Nonetheless, these effects have the potential to be incorporated in an automated DEM differencing processing chain if/when their corrections reach maturity of automated implementation. Alternately, they may be bundled into one co-registration adjustment, such as that applied by Miller et al.

(2008) which may be important for DEM differencing with DEMs made from historical imagery (Künz et al. 2012). Using the selected co-registration method they imply a manual intervention step essential for proper assessment of glacier mass changes from DEM differencing.

The final post processing procedures include error estimation for the glacier elevation change measurements. We rely on statistical error modeling using estimates based upon the selected stable terrain assuming that the elevation measurement technique behaves similarly on and off glaciers, which in some cases (i.e. optical photogrammetry) may not be completely true. After co-registration, the random error of individual elevation changes may be estimated from standard deviation of the differences over stable terrain. Although rare, an alternate to using stable terrain is to analyze two DEMs on glaciers (or a DEM with laser altimetry, i.e. ICESat) acquired at the same time (Berthier et al., 2012). In addition to the random error estimation, the error of the mean vertical bias adjustment should be included in the total error budget. This uncertainty may be estimated by the triangulation residual of the co-registration vectors (see e.g. Nuth et al., 2012) or through a "null" test if two DEMs acquired at the same time are available (Berthier et al., 2012). Slope distributions of the terrain and elevation blunders in the DEMs may affect these estimates and should also be considered. For error estimates on mean glacier elevation changes and subsequent volume change estimates, spatial autocorrelation of the elevation data must be considered (Kääb, 2008; Rolstad et al., 2009).

# 4. Glacier elevation changes from repeat-pass altimetry

### 4.1 Background and previous works

The repeat-pass satellite altimetry is an alternative technique for estimating glacier elevation changes. There are two basic approaches: 1) the repeat-track method is based on single-cycle elevation differences which are computed at ground tracks of repeated satellite orbits (Pritchard et al., 2009); 2) the cross over method is based on dual-cycle elevation differences which are computed at crossing points of satellite altimeter orbit ground tracks (Zwally et al. 1989, Wingham et al. 1998). The cross-over method offers the most accurate observation of elevation trends, because the calculation is not dependent upon spatial variations in topography as repeat measurements are recorded from the same location in space. However, the data from past satellite missions (ERS, Envisat, ICESat) are sparsely distributed in space due to constraints of the mission ground tracks, and are best suited to studying changes over large ($>10^2$ km$^2$) areas (Nuth et al., 2010; Moholdt et al., 2010; Kääb et al., 2012). Data from the Envisat radar altimeter has been designed and demonstrated to operate with improved success over regions of rugged terrain (Roca et al., 2009), and data from the CryoSAT-2 satellite offer the potential for vastly superior spatial sampling due to the instruments finer ground-resolution and dense orbit ground track. For comparison, at a lattitude of 60º the average separation of ICESat, ERS/Envisat, and CryoSat orbit crossing points (where elevation trends may be determined) is 175 km, 35 km, and 2 km, respectively.

Although the technique of repeat-track altimetry provides measurements of elevation change that are of inferior accuracy to those acquired by the cross over method (due mainly to uncertainties of the spatial variation in ground topography as the orbit tracks do not exactly repeat), the approach provides a far greater density of spatial sampling because measurements are available in-between each dual-cycle cross over point. Single-cycle elevation differences can be obtained either by applying a slope correction to along-track data using local DEM

information or by fitting sloped-planes to data acquired between repeat altimeter ground tracks, or by differencing to a reference DEM (Moholdt et al., 2010; Rinne et al., 2011, Kääb et al., 2012). The basic algorithms for the three methods are well developed and have been widely reported in the literature (e.g. Zwally et al., 1989; Wingham et al., 1998; Shepherd et al., 2001; Shepherd and Wingham, 2007; Kääb, 2008, Kääb et al., 2012; Nuth et al., 2010; Moholdt et al., 2010). Their results have been compared during the Round Robin experiment of the project with the aim to select the 'best' performing algorithm. A validation activity using airborne measurement has also been performed.

The test site areas have been chosen trying to cover different sets of glacier sites, including critical areas, such as glaciers with rough surface. Two are the test sites considered: the Devon Ice Cap, on Devon Island in Nunavut arctic Canada, and the Austfonna Icecap, in Nordauslandet the Svalbard archipelago. The exercises were based both on laser and radar altimetry data. In particular, laser altimeter data have been used as input to the different implementations of the repeat-track method, whereas radar altimeter data have been used as input of the cross-over method. The laser data are the ones acquired by the ICESat/GLAS instrument during the full acquisition period (2003-2009). In particular the GLA06 level 1B elevation data have been used, which provide surface elevation already corrected from the geodetic and atmospheric effects and geolocated to the centre of the laser footprint. On the other hand, the radar data refer to the measurements acquired by the Envisat-RA2 altimeter during the period 2002-2010. The product used were the level 2 GDR.

### 4.2 Main Processing

As already mentioned in the previous section, the methods used in the round robin experiments were the cross-over method and the repeat-track method. For the former, the dual cross over algorithm reported in Wingham et al. (1998) has been applied (XO-RepAlt). Instead of combining ascending and descending tracks from a single orbital cycle, the elevation measurements from pairs of orbital cycles, acquired at two distinct times $t_1$ and $t_2$ are compared. In this manner two pairs of elevations can be considered and used for computing the elevation change: the ascending track elevation measured during orbit cycle 1 at time $t = t_1$ and the descending track elevation measured during orbit cycle 2 at time $t = t_2$, as well as the ascending track measured at the orbit cycle 2 and the descending track measured at orbit cycle 1 (the elevation change during one orbit cycle is supposed to be negligible).

For the repeat-track method, three different algorithms were considered: (1) the DEM-Projected correction method (DP-RT-RepAlt), described in Mohold et al, 2010 (a and b), is based on the projection of one profile onto a neighbouring one by accounting for the cross-track slope using an external DEM; elevations are then compared at each DEM-projected point by linear interpolation between the two closest footprints in the other profile; (2) the Rectangular Plane fitting method (RP-Rt-RepAlt), described in detail by Mohold et al. (2010 b), is based on a least-squares regression technique that fits rectangular planes to segments of repeat-track data; for each plane the elevation change rate, supposed constant, is estimated; and (3) the DEM Subtracting method (DS-RT-RepAlt), described in Ticconi et al. (2012), computes the difference between the altimetry measured elevations and the DEM elevations at each altimetry footprint location; the DEM elevations at these locations are obtained by interpolating the surrounding DEM values (see also Kääb, 2008; Kääb et al., 2012; Nuth et al., 2010).

The aims of the Round Robin were the validation of different repeat-pass altimetry algorithms for product generation, and the selection of a 'best' performing algorithm. The validation of the elevation change focused on: (a) comparison of temporally consistent airborne elevation changes with satellite altimeter elevation changes, (b) comparison of elevation changes derived from different sensors (e.g. radar vs. laser), and (c) comparison of elevation changes derived from different algorithms (cross-track vs. repeat track). The validation strategy (a) ensures independence, since it is based on external data which have not been used during the generation of the elevation change products derived from satellite altimeter data. The validation strategy (b) provides two independent elevation change products to be compared, because even if the same algorithm has been used to create them, it has been applied on two different data sets acquired by two different sensors. The same applies for the validation strategy (c), which provides two independent elevation change products derived from two different algorithms to a data set acquired by the same sensor.

The validation criteria were based upon the computation of the RMSE and the correlation coefficient R. This has been applied to the comparisons (a), (b) and (c) described above. The limitation of the cross over methods in terms of spatial coverage when compared with the repeat-track method has been shown in Ticconi et al. (2012) for the Devon Ice Cap. The authors compared the elevation changes obtained using the full ICESat/GLAS archive (20003-2009) and computed by applying the RP-RT-RepAlt with the elevation changes obtained using the Envisat radar altimeter data over the period 2002-2010 and applying the cross over method. The small number of cross over points spotted over the test site made these results unsuitable for the comparison of the different algorithms. On the other hand, the comparison between the different repeat-track implementations (DP-RT-RepAlt and RP-RT-RepAlt) is shown over the Ausftonna Ice Cap in Fig. 6. The good agreement between them, expressed by the correlation coefficient and the RMSE, indicates their almost equivalence.

*Figure 6*

From the validation against airborne data, it appeared that due to the large footprint the radar altimeter data were not measuring properly the elevation in correspondence of the ice sheet margin where slopes are steep. This is clearly shown in Fig. 7 where the absolute differences between the *dh/dt* trend obtained from airborne measurements and the ones obtained using the DP-RT-RepAlt, the RP-RT-RepAlt and the XO-RepAlt are plotted as function of the elevation. They show similar trends when the elevation becomes greater than 300 m. For elevation below this value, a dissimilarity between the absolute differences can be noted when the radar data are used, indicating that the radar performs better on regions with moderate slope than regions with high slope like the ice margin. Unfortunately, at these regions the validation dataset is unlikely to be representative. In addition, the repeat-track method applied to laser altimeter data provided estimates of surface elevation change with greater accuracy than the cross-over method applied to radar altimeter (Fig. 8).

*Figurse 7 and 8*

The selection of the best performing algorithm was based on the following criteria:

- spatial density of satellite derived surface elevation changes
- spatial coverage of satellite derived surface elevation changes
- temporal density of satellite derived surface elevation changes

- absolute accuracy relative to validation data
- processing time and manual interaction

Table 2 summarises the overall performance of the tested algorithms in relation to these selection criteria over the two test sites. The algorithm performance in relation to absolute accuracy is detailed in Table 3.

*Tables 2 and 3*

The comparison of the elevation change trends derived from satellite repeat altimetry has been made on the absolute differences of the elevation change maps. The root mean square error, RMSE, and the correlation coefficient, R, have been computed to provide a quantitative analysis. The results show that the DP-RT-RepAlt and the RP-RT-RepAlt algorithms have an RMSE of about 0.4 m/yr when compared with the airborne data indicating a good agreement and a result comparable with the estimated measurement accuracy. The good agreement with airborne data is confirmed also by the good value of the correlation coefficient (around 0.73). In addition, the two repeat track algorithms demonstrate a RMSE of the same order when inter-compared and a really high correlation coefficient (0.89), indicating that they are almost equivalent. Also the DS-RT-RepAlt algorithm shows a RMSE of the same order when compared with the RP-RT-RepAlt algorithm. Thus, it can be concluded that the three repeat algorithms investigated are almost equivalent.

## 5. Glacier velocity

### 5.1 Background and previous works

A large number of archived and upcoming optical and SAR satellite missions make it possible to operationally map and monitor glacier flow on a nearly global scale, providing unique glaciological information (Rignot et al., 2011; Heid and Kääb, 2012a and b). Such knowledge will provide a better understanding of a wide range of processes related to glacier dynamics, for example on glacier mass flux, flow modes and flow instabilities (e.g. surges), subglacial processes (e.g. erosion), supra- and intra-glacial mass transport, and the development of glacier lakes and associated hazards (Kääb et al., 2005). The comparison of the spatio-temporal variations of glacier velocities both within and between regions will improve understanding of climate change impacts (e.g. Scherler et al., 2011). In this regard, mapping and monitoring glacier flow globally complements the possibilities for determination of glacier areas and volume changes described above.

The calculation of glacier velocity fields is possible with repeat optical satellite imagery and SAR data using feature tracking methods. They are usually called “image matching” in the optical domain and “offset-tracking” in the microwave domain, but we here use the term offset-racking for both optical or SAR data. Indeed, strictly speaking image matching refers only to the image correlation itself and does not include the required pre- and post-processing procedures. The suitable temporal baselines of the repeat data are within two fundamental constraints: (i) the displacements have to exceed the accuracy of the method, i.e. have to be statistically significant; (ii) the surface changes such as melt, deformation, snow fall, etc. over the measurement period have to be small enough so that corresponding intensity or phase features can be matched in both data sets. Typical baselines suitable for optical data are weeks to years and days to a few weeks for SAR offset-tracking. Interferometric techniques are not

analyzed here as they require a very short baseline (days) and are less suitable for operational and global-scale application. However, SAR interferometry was widely used to determine flow velocities of ice sheets, where decorrelation due to a change of surface properties is less of a problem (e.g. Goldstein et al., 1993; Joughin et al., 1996; Rignot et al., 1997). To overcome signal decorrelation when using longer time intervals or more quickly changing temperate glaciers, offset-tracking procedures are also largely adopted (Gray et al., 1998; Michel and Rignot, 1999; Derauw, 1999; Strozzi et al., 2002; Rignot et al., 2011). Repeat optical satellite imagery from sensors such as SPOT, ASTER and Landsat ETM+ pan was also widely applied to determine flow velocities of glaciers (e.g. Berthier et al., 2005; Herman et al., 2011; Kääb, 2005b; Kääb et al. 2006; Scherler et al., 2008 and 2011). Here we focus on Landsat data with 15 m spatial resolution (ETM+ pan), due mainly to the large spatial coverage of one scene, the huge archive available and future missions with similar characteristics (e.g. LDCM, Sentinel-2). Envisat ASAR, ALOS PALSAR and TerraSAR-X data were considered as typical microwave imagery for algorithm testing.

Despite their wide application, only few systematic studies exist that compare different algorithms and procedures for glacier surface velocity estimation based on repeat optical or microwave data, though some more give hints on tests and reasons for algorithm selection. Starting with optical sensors, Heid and Kääb (2012a) compared a number of frequently used and already published matching algorithms. Despite differences in the results under conditions that are initially difficult, for instance in areas with low visual contrast, most algorithms are in principle able to measure displacements at sub-pixel precision. As most optical offset tracking procedures rely on matching repeat orthoimages, errors in the sensor model, sensor orientation, and the DEM used translate into lateral errors in the data to be matched and thus in the displacements obtained. Leprince et al. (2007) developed a procedure to rigorously remove such effects and Debella-Gilo and Kääb (2011) analyse the effect of a locally adaptive way to determine the optimal size of matching templates, combined with finding suitable matching targets based on the image grey scale variations (image signal-to-noise ratio). Ahn and Howat (2011) applied normalized cross-correlation (NCC) to a large number of input image versions (e.g. channels, gradients, filtered versions, principle components) and a range of template sizes, to find the most probable displacement based on the resulting stack. Though computationally very expensive, this approach is locally adaptive in many geometric and radiometric respects. In the same direction Liu et al. (2012) propose a multi-scale matching process to overcome the dependence of the matching window size on the velocity. For SAR data comparisons are related to optical versus SAR methods and the impact on the matching window size on the derived velocity (Huang and Li, 2011) or InSAR versus offset (or speckle) tracking methods (e.g. Joughin, 2002; Luckmann et al., 2007).

In the round robin for the glacier velocity product different algorithms for SAR and optical data were compared with robust and global-scale applications in mind. Test regions were located in Iceland (Breidamerkurjökull), Himalaya (Baltoro glacier in the Karakoram), and Svalbard (Vestfonna Ice Cap). In following sections, we describe the algorithms selected for generating the glacier velocity product, including practical considerations during the pre- and post-processing stages.

*Figure 9*

**5.2 Pre-processing for SAR and optical sensors**

In the pre-processing step data import and quality checks (e.g. missing line detection for SAR data) are performed. The most crucial step is then the accurate co-registration of the data to be

matched. Offsets measured using the same algorithms as the main processing (though often with different parameterizations, e.g. with a reduced sampling to decrease the computational effort) or using another algorithm form the base of co-registration. A glacier outline mask and a DEM can be optionally employed to limit the search over stable ground and to compensate for the stereo offsets relevant for the range offset field, respectively. The search (= slave) image can be then either transformed to the geometry of the reference (= master) image or (e.g. polynomial) transformation parameters can be computed and applied to the matching results without transforming the images. The co-registration transformation has the advantage to make offset-tracking and other usages of the images easier, but increases the computational time and storage and may introduce loss of information, even if this is marginal for SAR data.

A generic optical offset-tracking procedure for large-scale and frequent operational usage will have to be based on orthorectified data, as some data are only available in orthorectified form (Landsat, Sentinel-2) or because orthorectification within the tracking procedure will be difficult, e.g. due to instable sensor geometry (Leprince et al. 2007). As a result, the eventually resulting displacements are not necessarily the highest accuracy level theoretically achievable, but will rather be contaminated by propagated DEM errors, errors in the sensor model and sensor orientation, such as jitter (Nuth and Kääb, 2011). Co-registration can in some cases partially reduce these influences empirically, but will in most cases typically rather be useful to estimate the size of these effects and add them to the error budget of the displacements. Care is for instance necessary when assuming that off-glacier DEM errors, as visible through non-zero stable ground offsets, are equally valid for glacier surfaces and elevations over glaciers can, in contrast to off-glacier terrain, be massively outdated due to glacier thickness changes.

### 5.3 Main Processing of satellite optical data

For the round robin we have applied several algorithms to the same data sets. For an internal algorithm test we have selected from the six algorithms discussed in Heid and Kääb (2012a), those two which are assumed to be beneficial for large-scale, operational offset tracking and compared them to algorithms (3) and (4) applied by the external round robin participants:

(1) normalized cross-correlation (NCC) in the spatial domain;
(2) orientation correlation (CCF-O) in the frequency domain;
(3) a modified version of the GAMMA software (matching template 30x30 pixels, 5-pixel spacing) using in principle NCC for offset tracking, but solved in the Fourier domain;
(4) a modification of the Ahn and Howat (2011) method using NCC (matching template 31x31 pixels, 8-pixel spacing) but sophisticated pre- and post-processing procedures.

As Fig. 10 shows, the NCC method performs similar to the CCF-O in areas with good visual contrast, but obtains fewer correct matches in areas with low visual contrast. The Fourier methods (2) and (3) performed also similarly in areas of high visual contrast but fewer correct matches are obtained by (3) in areas of low visual contrast. This is expected since the method is based on NCC that has worse performance in low contrast areas. For areas in which the velocity gradients (strain rates) are large, the NCC (1) seems to outperform both of the Fourier methods tested. Significant variation in the results may be obtained through advanced pre- and post- processing procedures. For example, it seems that more correct matches are obtained over Biafo glacier compared to (2) and (3). However, if only points inside a glacier mask are selected, some of the smaller glaciers, stagnant glacier fronts and large parts of the accumulation area, where the movement is slow, are neglected and unmatched.

*Fig. 10*

Results with satellite optical data suggest that no one matching method clearly outperforms all other methods investigated under all circumstances, but rather that a set of two methods – e.g. (1) and (2) – should be combined depending on the image conditions and the glacier characteristics. These two algorithms are chosen for further development in Glaciers_cci (see Appendix for equations). The algorithm evaluation further revealed that most algorithms and implementations are in principle able to achieve precisions in the sub-pixel range (e.g. if data taken from the same orbit are used).

**5.4 Main Processing of satellite SAR data**

The NCC algorithm is simple and robust and can also be applied to SAR data. Offsets are measured using patches that are M1 x M2 (range x azimuth) pixels at a set of positions in the scene. The locations may be uniformly distributed over the image frame but for deformation mapping at specific regions (i.e. glaciers) can be also selected for dense sampling. After global co-registration, the residual offsets should not be larger than a small fraction of the patch size that will be used for measuring the offset field. Typical values for M1 and M2 are in the range of 64 to 256 depending on the noise level, sensor resolution and specific application. Data covering the patch is extracted from each SLC and the patch SLC data might be over-sampled by a factor of 2 or more using FFT interpolation to substantially improve the accuracy (Werner et al., 2005). The location of the maximum of the 2D correlation function yields the desired range and azimuth offsets. In order to obtain an accurate estimate of the correlation peak, the correlation function values over a (m1 x m2) region can be fitted using a bi-quadratic polynomial surface. The SNR of the offset measurement is obtained by taking the ratio of the peak value divided by the average correlation level outside the (m1 x m2) peak region. Typical values for m1 and m2 are in the order 3. The implementation of the algorithms may vary significantly with regard to matching window sizes and oversampling factors and various pre- and post-processing routines may affect the quality of the results (Fig. 11). Because this method operates in the spatial domain (as a convolution operation), the computation is time-consuming, i.e. up to a few hours depending on window size, pixels spacing and oversampling factor.

*Figure 11*

The accuracy of the cross-correlation algorithm in a typical application over glaciers was investigated in various aspects, including a formal description of the error terms (noise, stereo offsets, not perfectly compensated satellite orbit configurations, ionospheric effects), matching on stable ground (Fig. 12a), inferring statistical errors on the difference of matching image 1 with image 2 with respect to the matching of image 2 with image 1, comparison against results from image data of equal or better resolution, and ground-based measurements from DGPS (Fig. 12b). We finally estimate the reliability of the cross-correlation algorithm to return co-registration parameters on the order of 1/10th of a SAR image pixel. This corresponds for the ALOS PALSAR and TerraSAR-X data separated by a temporal interval of 46 and 11 days, respectively, to an accuracy of about 10 m/yr and for the ENVISAT ASAR data separated by a temporal interval of 35 days to an accuracy of about 20 m/yr. Outliers are however frequent and require special attention in post-processing.

*Figure 12*

### 5.5 Post-processing

The matching algorithms do not directly provide perfect results including only accurate and reliable results. Errors and outliers cannot be avoided because of non-perfect image and ground conditions and have to be detected and filtered as much as possible in a post-processing step. The NCC algorithm provides, together with the offset with highest score, the correlation coefficient (CC) or signal-to-noise ratio (SNR) of the resulting offset. This measure can directly be used to estimate the potential quality of a match, and filters based on CC or SNR thresholds can be developed. Since CC and SNR, however, depend not only on the quality of a match but also on the image texture, such filters are not strictly conclusive and should be used with care and only in combination with other post-processing measures. The resulting displacement field can be low-pass filtered (e.g. mean, median, Gaussian, etc.) to filter out individual outliers. Similar to a resolution pyramid, the raw displacements can be compared to a low-pass filtered version of the field and measurements marked as outliers when the difference exceed a given threshold on displacement magnitude and direction (Heid and Kääb, 2012a). This procedure is very successful over dense fields, but may fail where successful matches are only scattered, or where entire groups of displacements have a similar bias.

Geometric constraints such as maximum magnitude or direction sectors can be also used as filters. However, they are not very useful for large-scale applications including a number of glaciers with different speeds and orientations. Also, for instance, gradients in glacier velocities could be used to filter, but they are very different from region to region due to the large variety of glaciers. To filter the displacements based, for instance, on the assumption that glaciers flow down-slope is considered to be impossible globally, because the required accurate elevation models are not available in all glacierized areas, and because of physical reasons where this assumption does not simply hold, such as in confluence areas or for supraglacial ice topography. The comparison of results using different pre-processing techniques or using CCF-O and NCC results can be as well useful in reducing erroneous measurements.

It should finally be noted that in our opinion glaciologically sound and useful glacier displacements can only be obtained when the automatic results undergo an expert check and, potentially, editing (similar to the well acknowledged and good practice in multispectral glacier mapping). Thus, the aim of displacement filters is to support the analyst in removing the obvious errors as much as possible to focus on details that require glaciological expert judgement. Ahn and Howat (2011) showed that also the (automated) comparison of results using different pre-processing techniques can be useful, in particular in reducing erroneous measurements. However, as the CCF-O has an inherent bi-directional gradient filter, comparison of its results to NCC results resembles to some extent also the comparison of differently pre-processed images.

## 6. Discussion

### 6.1 Glacier area

Deriving glacier outlines from multispectral (optical) satellite images is straightforward from any of the available algorithms given that snow and cloud conditions allow it. Manually selecting and optimizing classification thresholds has the advantage of minimizing the

workload for editing in the post-processing stage (e.g. in shadow regions), but differences in the mapped glacier area when using a fixed threshold will be small in regions with only few regions in shadow. On the other hand, correction of debris-covered glacier regions remain a laborious task. Although further semi-automated methods have been proposed recently (e.g. Bhambri et al., 2011; Shukla et al., 2011; Atwoodet al., 2010; Frey et al., 2012) they are all not in a stage where the automatically derived outlines have the required accuracy, i.e. manual corrections have to be applied in any case. Nonetheless they provide valuable support for deciding where glacier outlines should be. Actually, this decision can even in the field and with support from geophysical techniques be difficult. For the time being it might be worthwile to prepare illustrated guidelines for the analyst, showing where glacier margins are located in difficult cases with examples from glaciers all around the world. At best, such a document is prepared by a larger community to have some consensus on it.

As a general conclusion, we propose that

- the satellite scenes to be processed are carefully selected in regard to snow and cloud conditions (mosaicing might be required),
- automated methods are used to map the bare ice,
- the threshold values are chosen in a region with cast shadow,
- correction of the debris-covered parts considers all information available (e.g. results of an automatic algorithm, hillshades from DEMs, high-resolution imagery in Google Earth™ or similar tools, discussion with colleagues, following examples and guidelines).

### 6.2 Elevation change from DEM differencing

The Glaciers_cci project focuses on the initial generation of an automatic processing scheme for glacier elevation changes from multi-temporal DEM differencing. The first step towards automated DEM differencing is implementation of a universal co-registration algorithm. The present round robin tested three automated approaches and all of them performed with similar accuracies but different efficiencies. In terms of universal application, we choose a co-registration algorithm based upon terrain slope and aspect that requires not more than 2-3 iterations and is applicable with non-continuous elevation data, for example, from ICESat. Other lessons learned from the round robin are that various software products have different importing routines for the same file format (i.e. Geotiff) affecting the pixel definition (pixel centre vs. corner) and leading to large co-registration errors (typically half a pixel size) if an algorithm implementation requires switching the software. Thus, an automated processing chain for DEM differences should be maintained within one software product.

Apart from these challenges, results from the round robin for co-registering DEMs shows that sub-pixel accuracies are easily obtainable using the three tested automatic algorithms. Only the analytical method using slope/aspect works well with non-continuous data, such as from ICESat and can be solved with a minimum of iterations. This is in contrast to other methods which require hundreds to thousands of iterations. Nonetheless, the analytical solution requires the availability of stable terrain, typically with a uniform distribution of aspects on steeper slopes. While this is the case for the majority of the glacierized regions in the world, it may not work for regions without stable terrain and/or where only very low slope surfaces are available as the equation is not defined for a zero slope. Actually, the vertical co-registration adjustment has the largest variability between the methods applied in the round robin (Table 2) and this might be related to the selection of stable terrain. Its characteristics might thus have large impacts on the co-registration parameters solved as well as for any error quantification based upon this terrain.

### 6.3 Elevation changes from altimetry

In regard to the comparison between the elevation changes derived with satellite altimetry and the airborne measurements, the absolute differences obtained using the DP-RT-RepAlt, the RP-RT-RepAlt and the XO-RepAlt show similar trends when the elevation becomes greater than 300 m. It evidently appeared that due to the large footprint the radar altimeter data were not measuring properly the elevation at the margin of the ice cap where slope is high. In addition, the repeat track method applied to laser altimeter data provided estimates of ice cap surface elevation change with significantly greater accuracy than the cross-over method applied to radar altimeter. The DS-RT-RepAlt method is the only one applicable for mid to low latitudes because of the large cross-track spacing between repeat tracks of up to several kilometres (Kääb et al., 2012). However, Kääb et al. (2012) also showed that even the SRTM DEM can be sufficient for this purpose. Table 5 summarises the overall performance of the tested algorithms in relation to the selection criteria described. Based on these results, the repeat-track method applied to laser altimeter data has been selected as the most reliable technique for developing satellite based observations of ice cap surface elevation change. It is worth underlining that the selected repeat-track algorithm is also applicable to new Cryosat-2 radar altimeter data, which are characterised by a footprint size comparable to the laser altimeter measurements. In addition, being the first satellite equipped with a SAR Interferometric Altimeter, it is able to point down the location of the echo on sloping surfaces, such as those found around the edges of ice caps.

*Table 5*

### 6.4 Glacier velocity

Results for glacier velocity measurement using satellite optical data suggest that no one matching method clearly outperforms all other methods investigated under all circumstances, but rather that a set of, for instance, two methods – e.g. the NCC and the CCF-O – should be combined depending on the image conditions and the glacier characteristics. Results from the round robin for SAR data demonstrated that the normalized cross-correlation of chips in amplitude SAR images performs better compared to the other SAR methods, in particular regarding its wider application to different glaciers and SAR data. Accuracy of offset-tracking using high to very-high SAR data with a time interval of one satellite cycle are about 10 m/yr, similar to the accuracy for medium-resolution optical satellite imagery (e.g. Landsat ETM+ pan) that is on the order of 15 m/year. However, there will be areas having better and also much less accuracy (e.g. outliers). The latter can occur due to:

- image co-registration and orthoprojection (can be checked over stable terrain);
- sub-pixel geometric sensor noise level (usually larger than algorithm precision);
- surface changes and transformations, e.g. influence of different illuminations and shift of surface features;
- mismatches due to similar but not corresponding features, e.g. self-similar ogives, crevasses or seracs, with errors of many pixels possible;
- ability of post-processing procedures to eliminate measurement noise and mismatches.

## 7. Conclusions and Perspectives

We have described methods and algorithms for deriving a range of glacier related products (extent, elevation changes, velocity fields) from a large variety of space-borne sensors types (optical and microwave imagers or altimeters). They generally provide complimentary information and are thus particularly useful for glaciological research when combined. The presented algorithms were selected for data production in the Glaciers_cci project after careful evaluation and comparison with alternative methods. In regard to a more general data processing workflow, all methods selected have also product specific peculiarities. While for the glacier area product the mapping algorithm is very simple (band ratio with threshold) and the manual editing of wrong classifications (debris cover) in the post-processing stage drives product accuracy, the quality of the elevation change product (from DEM differencing) depends on the quality of the input DEMs, and on the use of a single software processing chain for co-registration (as pixel coordinates can be interpreted differently). Both products may require user interaction and inspection in a post-processing step. On the other hand, the processing of the velocity and elevation change (from altimetry) products is largely automatic, but the algorithms are much more complex and the computational resources required are thus much higher. In all cases product quality also depends on the quality of external data such as a high-quality DEM, which is not yet available for all high-mountain regions of the world. Moreover, if more than one algorithm can be applied (e.g. for velocity), the best choice often depends on the specific characteristics of the investigated region and might have to be tested. For ice velocities it is suggested that the major differences between different processing schemes stem to a large extent also from different implementations, pre- and post-processing steps, which should thus be carefully selected. It turned out, however, that velocity measurement from repeat satellite optical and SAR sensors has a large potential to be done automatically thus arriving at robust global-scale products. More detailed information on algorithms, work flows and product generation is available from the Glaciers_cci website (http://www.esa-glaciers-cci.org/). With the recently launched (Cryosat-2, TanDEM-X) or planned (Sentinels 1 and 2, LDCM) satellite missions and the commitment to free data distribution by space agencies, the contribution of space-borne sensors to glacier monitoring will play an increasing role in the future.

**Acknowledgements**

**Author contributions**

FP lead the overall writing and
xxx participated in the rr for xx
xxx participated in the rr for xx
and xxx participated in the rr for xx
RR participant altimetry:

## Appendix

The NCC is given by:

$$CC(i,j) = \frac{\sum_{k,l}(s(i+k,j+l)-\mu_s)(r(k,l)-\mu_r)}{\sqrt{\sum_{k,l}(s(i+k,j+l)-\mu_s)^2 \sum_{k,l}(r(k,l)-\mu_r)^2}}$$

where $(i,j)$ indicates the position in the search area, $(k,l)$ the position in the reference area, $r$ the pixel value of the reference chip, $s$ the pixel value of the search chip, $\mu_r$ the average pixel value of the reference chip and $\mu_s$ the average pixel value of the search chip.

In CCF-O, orientation images are first derived from the original images. Taking f(x,y) as the image at time t = 1 and g as the image at time t = 2, the orientation images $f_o$ and $g_o$ are created from:

$$f_o(x,y) = sgn\left(\frac{\partial f(x,y)}{\partial x} + i\frac{\partial f(x,y)}{\partial y}\right)$$

$$g_o(x,y) = sgn\left(\frac{\partial g(x,y)}{\partial x} + i\frac{\partial g(x,y)}{\partial y}\right)$$

$$\text{where } sgn(x) = \begin{cases} 0 & \text{if } |x| = 0 \\ \frac{x}{|x|} & \text{otherwise} \end{cases}$$

where *sgn* is the signum function, $i$ is the complex imaginary unit, and the new images $f_0$ and $g_0$ are complex, are matched using cross-correlation:

$$CC(i,j) = IFFT\left(F(u,v)G^*(u,v)\right)$$

Here $F(u,v)$ is the Fast Fourier Transform (FFT) of the matching window from the image at time t = 1, $G(u,v)$ is the FFT of the matching window from the image at time t = 2, * denotes the complex conjugated and IFFT is the Inverse Fast Fourier Transform.

## References


Ahn, Y. and Howat, I.M. (2011): Efficient automated glacier surface velocity measurement from repeat images using multi-image/multichip and null exclusion feature tracking. IEEE Transactions on Geoscience and Remote Sensing, 49 (8), 2838-2846.

Albert, T.H. (2002): Evaluation of remote sensing techniques for ice-area classification applied to the tropical Quelccaya Ice Cap, Peru. Polar Geography, 26 (3), 210-226.

Andreassen, L.M., Paul, F., Kääb, A. and Hausberg, J.E. (2008): Landsat-derived glacier inventory for Jotunheimen, Norway, and deduced glacier changes since the 1930s. The Cryosphere, 2, 131-145.

Aniya, M., Sato, H., Naruse, R., Skvarca, P. and Casassa, G. (1996): The use of satellite and airborne imagery to inventory outlet glaciers of the Southern Patagonia Icefield, South America. Photogrammetric Engineering and Remote Sensing, 62, 1361 - 1369.

Arendt, A., and 77 others (2012): Randolph glacier inventory [v2.0]: A dataset of global glacier outlines. GLIMS Technical report, 35 pp. Online at: http://www.glims.org/RGI, Global Land Ice Measurements from Space, Boulder, Colorado, USA.

Atwood, D., Meyer, F. and Arendt, A. (2010): Using L-band SAR coherence to delineate glacier extent. Canadian Journal of Remote Sensing, 36, S186-S195.

Bajracharya, S.R., and B.R. Shrestha (Eds.) (2011): The status of glaciers in the Hindu Kush-Himalayan Region, ICIMOD, Kathmandu.

Bayr, K. J., Hall, D. K. and Kovalick, W. M. (1994): Observations on glaciers in the eastern Austrian Alps using satellite data. International Journal of Remote Sensing, 15 (9), 1733-1742.

Berthier, E., Vadon, H., Baratoux, D., Arnaud, Y., Vincent, C., Feigl, K.L., Remy, F. and Legresy, B. (2005): Surface motion of mountain glaciers derived from satellite optical imagery. Remote Sensing of Environment, 95, 14-28.

Berthier, E., Arnaud, Y., Vincent, C., and Rémy, F. (2006). Biases of SRTM in high-mountain areas: Implications for the monitoring of glacier volume changes. Geophysical Research Letters, 33 (8).

Berthier, E., Arnaud, Y., Kumar, R., Ahmad, S., Wagnon, P., and Chevallier, P. (2007). Remote sensing estimates of glacier mass balances in the Himachal Pradesh (Western Himalaya, India). Remote Sensing of Environment, 108(3), 327-338.

Berthier, E., Schiefer, E., Clarke, G. K. C., Menounos, B., and Remy, F. (2010). Contribution of Alaskan glaciers to sea-level rise derived from satellite imagery. Nature Geoscience, 3(2), 92-95.

Berthier, E., Scambos, T. A., and Shuman, C. A. (2012). Mass loss of Larsen B tributary glaciers (Antarctic Peninsula) unabated since 2002. Geophysical Research Letters, 39(13), L13501.

Bhambri, R., Bolch, T. and Chaujar, R.K. (2011): Automated mapping of debris-covered glaciers in the Garhwal Himalayas using ASTER DEMs and multi-spectral data. International Journal of Remote Sensing, 32 (23), 8095-8119.

Bolch, T., Buchroithner, M., Pieczonka, T. and Kunert, A. (2008): Planimetric and volumetric glacier changes in the Khumbu Himal, Nepal, since 1962 using Corona, Landsat TM and ASTER data. Journal of Glaciology, 54, 592-600.

Bolch, T., Menounos, B., Wheate, R. (2010): Landsat-based glacier inventory of western Canada, 1985-2005. Remote Sensing of Environment, 114 (1), 127-137.

Cox, L. H., and March, R. S. (2004). Comparison of geodetic and glaciological mass-balance techniques, Gulkana Glacier, Alaska, USA. Journal of Glaciology, 50 (170), 363-370.

Debella-Gilo, M. and Kääb, A. (2011): Locally adaptive template sizes in matching repeat images of Earth surface mass movements. ISPRS Journal of Photogrammetry and Remote Sensing, 69, 10-28.

Derauw, D. (1999): DInSAR and coherence tracking applied to glaciology: The example of Shirase Glacier. Proceedings FRINGE'99, Liège, Belgium.

Dozier, J. (1989): Spectral signature of alpine snow cover from Landsat 5 TM. Remote Sensing of Environment, 28, 9-22.

Finsterwalder, R. (1954). Photogrammetry and glacier research with special reference to glacier retreat in the eastern Alps. Journal of Glaciology, 2 (15), 306-314.

Frey, H., Paul, F. and Strozzi, T. (2012): Compilation of a glacier inventory for the western Himalayas from satellite data: Methods, challenges and results. Remote Sensing of Environment, 124, 832-843.

Fricker, H. A., Borsa, A., Minster, B., Carabajal, C., Quinn, K. and Bills, B. (2005): Assessment of ICESat performance at the Salar de Uyuni, Bolivia. Geophysical Research Letters, 32, L21S06.

Gardelle, J., Berthier, E., and Arnaud, Y. (2012a): Correspondence: Impact of resolution and radar penetration on glacier elevation changes computed from DEM differencing. Journal of Glaciology, 58 (208).

Gardelle, J., Berthier, E., and Arnaud, Y. (2012b): Slight mass gain of Karakoram glaciers in the early twenty-first century. Nature Geoscience, 5 (5), 322-325.

Gardner, A.S., G. Moholdt, B. Wouters, G.J. Wolken, D.O. Burgess, M.J. Sharp, J.G. Cogley, C. Braun and C. Labine (2011): Sharply increased mass loss from glaciers and ice caps in the Canadian Arctic Archipelago. Nature, 473(7347), 357-360.

Gjermundsen, E.F., Mathieu, R., Kääb, A., Chinn, T., Fitzharris, B. and Hagen, J.O. (2011): Assessment of multispectral glacier mapping methods and derivation of glacier area changes, 1978-2002, in the central Southern Alps, New Zealand, from ASTER satellite data, field survey and existing inventory data. Journal of Glaciology, 57 (204), 667-683.

Goldstein R., Engelhardt, H., Kamb, B., and Frolich R (1993): Satellite radar interferometry for monitoring ice sheet motion: application to an antarctic ice stream. Science, 262 (5139),1525-30.

Gray, L., Mattar, K. and Vachon, P. (1998): InSAR results from the RADARSAT Antarctic mapping mission: Estimation of glacier motion using a simple registration procedure. Proceedings. IGARSS'98, Seattle, WA.

Gruen, A. and Akca, D. (2005). Least squares 3D surface and curve matching. ISPRS Journal of Photogrammetry and Remote Sensing, 59 (3), 151-174.

Hall, D. K., Ormsby, J. P., Bindschadler, R. A. and Siddalingaiah, H. (1987): Characterization of snow and ice zones on glaciers using Landsat Thematic Mapper data, Annals of Glaciology, 9, 104-108.

Haug, T., Kääb, A. and Skvarca, P. (2010): Monitoring ice shelf velocities from repeat MODIS and Landsat data - a method study on the Larsen similar to C ice shelf, Antarctic Peninsula, and 10 other ice shelves around Antarctica. Cryosphere, 4 (2), 161-178.

Heid T. and Kääb A. (2012a): Evaluation of existing image matching methods for deriving glacier surface displacements globally from optical satellite imagery. Remote Sensing of Environment, 118, 339-355.

Heid T. and Kääb A. (2012b): Repeat optical satellite images reveal widespread and long term decrease in land-terminating glacier speeds. The Cryosphere, 6, 467-478.

Herman, F., B. Anderson and S. Leprince (2011): Mountain glacier velocity variation during a retreat/advance cycle quantified using sub-pixel analysis of ASTER images. Journal of Glaciology, 57 (202), 197-207.

Huang, L. and Li, Z. (2011): Comparison of SAR and optical data in deriving glacier velocity with feature tracking. International Journal of Remote Sensing, 32 (10), 2681-2698.

Jacobs, J. D., Simms, E. L. and Simms, A. (1997): Recession of the southern part of Barnes Ice Cap, Baffin Island, Canada, between 1961 and 1993, determined from digital mapping of Landsat TM. Journal of Glaciology, 43, 98-102.

Joerg, P. C., Morsdorf, F. and Zemp, M. (2012): Uncertainty assessment of multi-temporal airborne laser scanning data: A case study on an Alpine glacier. Remote Sensing of Environment, 127, 118-129.

Joughin, I. (2002): Ice-sheet velocity mapping: a combined interferometric and speckle-tracking approach. Annals of Glaciology, 34, 195-201.

Joughin, I., Tulaczyk, S., Fahnestock, M. and Kwok, R. (1996): A mini-surge on the Ryder Glacier, Greenland, observed by satellite radar interferometry. Science, 274, 228-230.

Joughin, I., Kwok, R., and Fahnestock M. (1998): Interferometric estimation of three-dimensional ice-flow using ascending and descending passes. IEEE Trans. Geosci. Remote Sensing, 36, 25-37.

Kääb, A. (2005a): Remote Sensing of Mountain Glaciers and Permafrost Creep. Schriftenreihe Physische Geographie, Geographisches Institut der Universität Zürich, 48, 266 pp.

Kääb, A. (2005b): Combination of SRTM3 and repeat ASTER data for deriving alpine glacier flow velocities in the Bhutan Himalaya. Remote Sens. Environm., 94 (4), 463-474.

Kääb A. (2008): Glacier volume changes using ASTER satellite stereo and ICESat GLAS laser altimetry. A test study on Edgeøya, Eastern Svalbard. IEEE Transactions on Geoscience and Remote Sensing, 46 (10), 2823-2830.

Kääb, A., Huggel, C., Fischer, L., Guex, S., Paul, F., Roer, I., Salzmann, N., Schlaefli, S., Schmutz, K., Schneider, D., Strozzi, T. and Weidmann, W. (2005): Remote sensing of glacier- and permafrost-related hazards in high mountains: an overview. Natural Hazards and Earth System Science, 5 (4), 527-554.

Kääb, A., Lefauconnier, B. and Melvold., K. (2006): Flow field of Kronebreen, Svalbard, using repeated Landsat 7 and ASTER data. Annals of Glaciology, 42(1), 7-13.

Kääb A. , E. Berthier, C. Nuth, J. Gardelle and Y. Arnaud. (2012): Contrasting patterns of early twenty-first-century glacier mass change in the Himalayas. Nature, 488 (7412), 495-498.

Kargel, J.S., M. J. Abrams, M. P. Bishop, A. Bush, G. Hamilton, H. Jiskoot, A. Kääb, H. H. Kieffer, E. M. Lee, F. Paul, F. Rau, B. Raup, J. F. Shroder, D. Soltesz, L. Stearns, R. Wessels and the GLIMS Consortium (2005): Multispectral imaging contributions to Global Land Ice Measurements from Space. Remote Sensing of Environment, 99, 187-219.

Kargel, J.S. and 15 others (2012): Greenland's shrinking ice cover: ″fast times″ but not that fast. The Cryosphere, 6, 533-537.

Kaser, G., J.G. Cogley, M.B. Dyurgerov, M.F. Meier and A. Ohmura (2006): Mass balance of glaciers and ice caps: Consensus estimates for 1961-2004. Geophys. Res. Lett., 33, L19501.

Korona, J., Berthier, E., Bernard, M., Rémy, F., and Thouvenot, E. (2009). SPIRIT. SPOT 5 stereoscopic survey of Polar Ice: Reference Images and Topographies during the fourth International Polar Year (2007-2009). ISPRS Journal of Photogrammetry and Remote Sensing, 64 (2), 204-212.

Kunz, M., M. A. King, J. P. Mills, P. E. Miller, A. J. Fox, D. G. Vaughan, and S. H. Marsh (2012),Multi-decadal glacier surface lowering in the Antarctic Peninsula. Geophys. Res. Lett., 39, L19502.

Larsen, C. F., Motyka, R. J., Arendt, A. A., Echelmeyer, K. A., and Geissler, P. E. (2007). Glacier changes in southeast Alaska and northwest British Columbia and contribution to sea level rise. Journal of Geophysical Research-Earth Surface, 112(F1), F01007.

Le Bris, R., Paul, F., Frey, H. and Bolch, T. (2011): A new satellite-derived glacier inventory for western Alaska. Annals of Glaciology, 52 (59), 135-143.

Lemke, P., J. Ren, R. Alley, I. Allison, J. Carrasco, G. Flato, Y. Fujii, G. Kaser, P. Mote, R. Thomas and T. Zhang (2007): Observations: change in snow, ice and frozen ground. Climate Change 2007: The Physical Science Basis. Contribution of Working Group I to the Fourth Assessment Report of the Intergovernmental Panel on Climate Change, S. Solomon, D. Qin, M. Manning, Z. Chen, M. Marquis, K.B. Averyt, M. Tignor and H.L. Miller, Eds., Cambridge University Press, Cambridge, 337-384.

Liu, H.X., Wang, L., Tang, S.J. and Jezek, K.C. (2012): Robust multi-scale image matching for deriving ice surface velocity field from sequential satellite images. International Journal of Remote Sensing, 33 (6) 1799-1822.

Luckman, A., Quincey, D. and Bevan, S. (2007): The potential of satellite radar interferometry and feature tracking for monitoring flow rates of Himalayan glaciers. Remote Sensing of Environment, 111, 172-181.

Malenovsky, Z., H. Rott, J. Cihlar, M E. Schaepman, G. García-Santos, R. Fernandes and M. Berger (2012): Sentinels for science: Potential of Sentinel-1, -2, and -3 missions for scientific observations of ocean, cryosphere, and land. Remote Sensing of Environment 120, 91-101.

Manley, W. F. (2008): Geospatial inventory and analysis of glaciers: a case study for the eastern Alaska Range. In Williams, R.S., Jr. and J.G. Ferrigno, eds. Satellite image atlas of glaciers of the world. USGS Professional Paper, 1386-K, K424-K439.

Miller, P. E., Kunz, M., Mills, J. P., King, M. A., Murray, T., James, T. D., and Marsh, S. H. (2009). Assessment of Glacier Volume Change Using ASTER-Based Surface Matching of Historical Photography. IEEE Transactions On Geoscience and Remote Sensing, 47(7), 1971-1979.

Miller, P. E., Mills, J., Edwards, S., Bryan, P., Marsh, S., Mitchell, H., and Hobbs, P. (2008). A robust surface matching technique for coastal geohazard assessment and management. ISPRS Journal of Photogrammetry and Remote Sensing, 63(5), 529-542.

Michel, R. and Rignot E. (1999): Flow of Glaciar Moreno, Argentina, from repeat-pass Shuttle Imaging Radar images: Comparison of the phase correlation method with radar interferometry. J. Glaciol., 45 (149), 93–100.

Moholdt, G., J.O. Hagen, T. Eiken and T.V. Schuler (2010a): Geometric changes and mass balance of the Austfonna ice cap, Svalbard. The Cryosphere, 4, 21-34.

Moholdt, G., C. Nuth, J.O. Hagen and J. Kohler (2010b): Recent elevation changes of Svalbard glaciers derived from ICESat laser altimetry. Remote Sensing of Environment, 114 (11), 2756-2767.

Mohr, J.J., Reeh, N. and Madsen S. (1998): Three-dimensional glacial flow and surface elevation measured with radar interferometry. Nature, 391, 273–276.

Nuth, C., and Kääb, A. (2011). Co-registration and bias corrections of satellite elevation data sets for quantifying glacier thickness change. The Cryosphere, 5(1), 271-290.

Nuth, C., Moholdt, G., Kohler, J., Hagen, J. O., and Kääb, A. (2010). Svalbard glacier elevation changes and contribution to sea level rise. Journal of Geophysical Research-Earth Surface, 115.

Nuth, C., Schuler, T. V., Kohler, J., Altena, B., and Hagen, J. O. (2012). Estimating the long-term calving flux of Kronebreen, Svalbard, from geodetic elevation changes and mass-balance modelling. Journal of Glaciology, 58 (207), 119-133.

Østrem, G. (1975): ERTS - 1 data in glaciology - an effort to monitor glacier mass balance from satellite imagery, Journal of Glaciology, 15, 403-415.

Paul, F. (2002): Changes in glacier area in Tyrol, Austria, between 1969 and 1992 derived from Landsat 5 TM and Austrian Glacier Inventory data. International Journal of Remote Sensing, 23 (4), 787-799.

Paul, F. (2008). Calculation of glacier elevation changes with SRTM: is there an elevation-dependent bias? Journal of Glaciology, 54 (188), 945-946.

Paul, F. and Kääb, A. (2005): Perspectives on the production of a glacier inventory from multispectral satellite data in the Canadian Arctic: Cumberland Peninsula, Baffin Island. Annals of Glaciology, 42, 59-66.

Paul, F. and W. Haeberli (2008): Spatial variability of glacier elevation changes in the Swiss Alps obtained from two digital elevation models. *Geophys. Res. Lett.*, 35, L21502.

Paul, F. and J. Hendriks (2010): *Optical remote sensing of glaciers*. In: Pellikka, P. and Rees, W.G (Eds.)., Remote Sensing of Glaciers. CRC Press, Taylor and Francis, Leiden, 137-152.

Paul, F., Kääb, A., Maisch, M., Kellenberger, T. W. and Haeberli, W. (2002): The new remote-sensing-derived Swiss glacier inventory: I. Methods. Annals of Glaciology, 34, 355-361.

Paul, F., Huggel, C., Kääb, A. and Kellenberger, T. (2003): Comparison of TM-derived glacier areas with higher resolution data sets. EARSeL Workshop on Remote Sensing of Land Ice and Snow, Bern, 11.-13.3.2002. EARSeL eProceedings, 2, 15-21.

Paul, F., R. Barry, G. Cogley, H. Frey, W. Haeberli, A. Ohmura, S. Ommanney, B. Raup, A. Rivera, M. Zemp (2009): Recommendations for the compilation of glacier inventory data from digital sources. Annals of Glaciology, 50 (53), 119-126.

Paul, F., H. Frey and R. Le Bris (2011): A new glacier inventory for the European Alps from Landsat TM scenes of 2003: Challenges and results. Ann. Glaciol., 52 (59), 144-152.

Paul, F., N. Barrand, E. Berthier, T. Bolch, K. Casey, H. Frey, S.P. Joshi, V. Konovalov, R. Le Bris, N. Mölg, G. Nosenko, C. Nuth, A. Pope, A. Racoviteanu, P. Rastner, B. Raup, K. Scharrer, S. Steffen and S. Winsvold (in press): On the accuracy of glacier outlines derived from remote sensing data. Annals of Glaciology, 54 (63).

Pohjola, V. A., Christoffersen, P., Kolondra, L., Moore, J. C., Pettersson, R., Schäfer, M., Strozzi, T., and Reijmer, C. H. (2011): Spatial distribution and change in the surface ice-velocity field of Vestfonna ice cap, Nordaustlandet, Svalbard, 1995–2010 using geodetic and satellite interferometry data, Geografiska Annaler: Series A, Physical Geography, 93, 323–335.

Pritchard, H.D., R.J. Arthern, D.G. Vaughan and L.A. Edwards (2009): Extensive dynamic thinning on the margins of the Greenland and Antarctic ice sheets. Nature, 461, 971-975.

Racoviteanu, A.E., M.W. Williams and R.G. Barry (2008): Optical remote sensing of glacier characteristics: A review with focus on the Himalaya. Sensors, 8, 3355-3383.

Racoviteanu, A.E, Paul, F., Raup, B., Khalsa, S.J.S. and Armstrong, R. (2009): Challenges in glacier mapping from space: recommendations from the Global Land Ice Measurements from Space (GLIMS) initiative. Annals of Glaciology, 50 (53), 53-69.

Rastner, P., T. Bolch, N. Mölg, H. Machguth and F. Paul (2012): The first complete glacier inventory for the whole of Greenland. The Cryosphere Discussions, 6, 2399-2436.

Raup, B.H. and Kahlsa, S.J.S. (2007): GLIMS Analysis Tutorial. NSIDC, Boulder, Colorado. (http://www.glims.org/MapsAndDocs/assets/GLIMS_Analysis_Tutorial_a4.pdf)

Raup, B.H., A. Racoviteanu, S.J.S. Khalsa, C. Helm, R. Armstrong, and Y. Arnaud (2007b): The GLIMS Geospatial Glacier Database: a new tool for studying glacier change. Global and Planetary Change, 56, 101-110.

Rignot, E., Gogineni, S., Krabill, W. and Ekholm, S. (1997): North and Northeast Greenland ice discharge from satellite radar interferometry. Science, 276, 934–937.
Rignot, E., J. Mouginot and B. Scheuchl (2011): Ice Flow of the Antarctic Ice Sheet. Science, 333 (6048): 1427-1430.
Rinne, E.J., A. Shepherd, S. Palmer, M.R. van den Broeke, A. Muir, J. Ettema and D. Wingham (2011): On the recent elevation changes at the Flade Isblink Ice Cap, northern Greenland. 2011. Journal of Geophysical Research, 116, F03024.
Roca, M., S. Laxon and C. Zelli (2009): The EnviSat RA-2 Instrument Design and Tracking Performance: IEEE Transactions on Geoscience and Remote Sensing, 47, 3489-3506.
Rodriguez, E., Morris, C. S., and Belz, J. E. (2006). A global assessment of the SRTM performance. Photogrammetric Engineering and Remote Sensing, 72 (3), 249-260.
Rolstad, C., Haug, T., and Denby, B. (2009). Spatially integrated geodetic glacier mass balance and its uncertainty based on geostatistical analysis: application to the western Svartisen ice cap, Norway. Journal of Glaciology, 55, 666-680.
Rott, H. (1976): Analyse der Schneeflächen auf Gletschern der Tiroler Zentralalpen aus Landsat Bildern. Zeitschrift für Gletscherkunde und Glazialgeologie, 12, 1-28.
Rott, H. (1994): Thematic studies in alpine areas by means of polarimetric SAR and optical imagery. Advances in Space Research, 14, 217 - 226.
Rott, H. and Markl, G. (1989): Improved snow and glacier monitoring by the Landsat Thematic Mapper, Proceedings of a workshop on Landsat Themaic Mapper applications, ESA, SP-1102, 3-12.
Scherler, D., Leprince, S. and Strecker, M.R. (2008): Glacier-surface velocities in alpine terrain from optical satellite imagery - Accuracy improvement and quality assessment. Remote Sensing of Environment, 112 (10), 3806-3819.
Scherler, D., Bookhagen, B. and Strecker, M.R. (2011): Spatially variable response of Himalayan glaciers to climate change affected by debris cover. Nature Geoscience, 4 (3), 156-159.
Schiefer, E., B. Menounos and R. Wheate (2007): Recent volume loss of British Columbian glaciers, Canada. Geophys. Res. Lett., 34, L16503.
Shangguan et al., 2009). Shepherd, A. and D. Wingham (2007): Recent sea-level contributions of the Antarctic and Greenland ice sheets: Science, 315, 1529-1532.
Shepherd, A., D.J.Wingham, J.A.D. Mansley and H.F.J. Corr (2001): Inland thinning of Pine Island Glacier, West Antarctica. Science, 291, 862-864.
Shukla, A., M.K. Arora and R.P. Gupta (2011): Synergistic approach for mapping debris-covered glaciers using optical-thermal remote sensing data with inputs from geomorphometric parameters. Remote Sensing of Environment, 114 (7), 1378-1387.
Sidjak and Wheate, 1999)Strozzi T., A. Luckman, T. Murray, U. Wegmüller and C. Werner (2002): Glacier motion estimation using SAR offset-tracking procedures. IEEE Trans. Geosc. Remote Sens., 40 (11), 2384-2391.
Ticconi, F., A. Shepherd, A. Muir, G. Mohold, E. Rinne and F. Paul (2012): Preliminary Results on Algorithm and Sensor Comparisons for the Estimation of Surface Elevation Changes over Ice Caps using Altimetry Data. 20 Years of Progress in Radar Altimetry Symposium, Venice, Italy.
VanLooy, J. A., & Forster, R. R. (2008). Glacial changes of five southwest British Columbia icefields, Canada, mid-1980s to 1999. Journal of Glaciology, 54(186), 469-478.
VanLooy, J. A. (2011). Analysis of elevation changes in relation to surface characteristics for six glaciers in Northern Labrador, Canada using advanced space-borne thermal emission and reflection radiometer imagery. Geocarto International, 26(3), 167-181.

Van Niel, T. G., McVicar, T. R., Li, L. T., Gallant, J. C., and Yang, Q. K. (2008). The impact of misregistration on SRTM and DEM image differences. Remote Sensing of Environment, 112(5), 2430-2442.

Werner, C., Wegmüller, U., Strozzi, T. and Wiesmann, A. (2005): Precision estimation of local offsets between SAR SLCs and detected SAR images. Proceedings of IGARSS 2005, Seoul, Korea.

Williams, R.S., Jr., Hall, D.K. and Benson, C.S. (1991): Analysis of glacier facies using satellite techniques, Journal of Glaciology, 37, 120 - 127.

Williams, R. S., Jr., Hall, D. K., Sigurdsson, O. and Chien, J. Y. L (1997): Comparisson of satellite-derived with ground-based measurements of the fluctuations of the margins of Vatnajökull, Iceland, 1973-1992. Annals of Glaciology, 24, 72 -80.

Willis, M. J., Melkonian, A. K., Pritchard, M. E., and Ramage, J. M. (2012). Ice loss rates at the Northern Patagonian Icefield derived using a decade of satellite remote sensing. Remote Sensing of Environment, 117(0), 184-198.

Wingham, D.J., A. Ridout, R. Scharroo, R. Arthern and Shum, C.K. (1998): Antarctic elevation change from 1992 to 1996. Science, 282, 456-458.

Wulder, M.A. J.G. Masek, W.B. Cohen, T.R. Loveland, C.E. Woodcock (2012): Opening the archive: How free data has enabled the science and monitoring promise of Landsat. Remote Sensing of Environment, 122, 2-10.

Zemp, M., Jansson, P., Holmlund, P., Gärtner-Roer, I., Koblet, T., Thee, P., and Haeberli, W. (2010). Reanalysis of multi-temporal aerial images of Storglaciären, Sweden (1959-1999); Part 2: Comparison of glaciological and volumetric mass balances. The Cryosphere, 4(3), 345-357.

Zwally, H.J., A.C. Brenner, J.A. Major, R.A. Bindschadler and Marsh, J.G. (1989): Growth of Greenland Ice-Sheet - Measurement. Science, 246, 1587-1589.

# Tables

*Table 1: Overview table of automatically generated DEMs, typically free of charge and with (quasi) global glacier coverage available. A myriad of other sources exist but may not offer off-the-shelf DEM products, have only local coverage and/or have purchasing charges. These include national elevation products, SPOT1-4, IKONOS, Worldview, Cartosat, Kompsat.*

| Data | Acquisition Type | Resolution | Time Period |
|---|---|---|---|
| SRTM | Radar interferometry | 30-90 m | February, 2000 |
| ASTER | Optical photogrammetry | 30 m | 2000-present |
| SPOT5-HRS (SPIRIT Products) | Optical photogrammetry | 20-40 m | 2002-present |
| TanDEM-X | Radar interferometry | 12 m | 2010-present |

*Table 2: Co-registration parameters from the three automatic algorithms tested: A is the robust surface matching, B is the brute-force iterative minimization of difference residuals and C is the analytical solution using slope/aspect. The last column of the table shows the triangulation residuals between the three DEMs. All methods result in sub-pixel accuracies. Also shown are co-registration parameters and triangulation residuals between two DEMs and the collection of ICESat altimetry available over the scenes.*

| DEM differences / Triangulation* | Method | ΔX | ΔY | ΔZ |
|---|---|---|---|---|
| 2000 - 2006 | A | 24.4 | 21.8 | 7.6 |
| | B | -5.6 | -50.8 | 2.5 |
| | C | 24.3 | 20.6 | 3.2 |
| 2000 - 2002 | A | -12.0 | -4.6 | -1.0 |
| | B | -41.1 | -24.5 | -4.6 |
| | C | -13.4 | -9.1 | -4.1 |
| 2002 - 2006 | A | -36.3 | -25.8 | -8.5 |
| | B | -38.0 | 25.4 | -4.9 |
| | C | -38.4 | -26.2 | -7.5 |
| 2000 - ICESat | A | 11.6 | -14.4 | -8.5 |
| | B | - | - | - |
| | C | -1.71 | -3.90 | -3.80 |
| 2006 - ICESat | A | 25.3 | 18.4 | 9.9 |
| | B | - | - | - |
| | C | 25.78 | 12.68 | -0.25 |
| 2000 - 2002 - 2006* | A | 0.1 | 0.6 | 0.1 |
| | B | -2.5 | -0.8 | 2.2 |
| | C | -0.6 | 3.5 | -0.2 |
| 2000 - 2006 - ICESat* | A | 10.7 | -11.0 | -10.8 |
| | B | - | - | - |
| | C | -3.09 | 3.99 | -0.35 |

*Table 3: Algorithm performances*

| | Algorithms applied over Devon Ice Cap | | | Algorithms applied over Austfonna Ice Cap | | |
|---|---|---|---|---|---|---|
| | **DS-RT-RepAlt** | **RP-RT-RepAlt** | **XO-RepAlt** | **DP-RT-RepAlt** | **RP-RT-RepAlt** | **XO-RepAlt** |
| Spatial density | 4% | 5% | < 1% | 5% | 5% | 2% |
| Spatial coverage | 75% | 75% | < 5% | 75% | 75% | 60% |
| Temporal density | 1.6 $year^{-1}$ | 1.6 $year^{-1}$ | 10 $year^{-1}$ | 1.6 $year^{-1}$ | 1.6 $year^{-1}$ | 10 $year^{-1}$ |
| CPU | < 1 h | < 1 h | 1 day | 1 h | 1 h | 1 day w |
| Manpower time | 0.5 day | 0.5 day | 1 week | 0.5 day | 0.5 day | 1 week |
| Accuracy | 0.40 m/yr | 0.40 m/yr | 0.50 m/yr | 1 m/yr | 0.3 m/yr | 50 cm/yr |

*Table 4: Summaries of the RMSE and the correlation coefficient R obtained from the validation activity.*

| RMSE (m/yr)/R | DS-RT-RepAlt (laser alt.) | DP-RT-RepAlt (laser alt.) | RP-RT-RepAlt (laser alt.) | XO-RepAlt (radar alt.) | airborne |
|---|---|---|---|---|---|
| DS-RT-RepAlt (laser alt.) | --- | N/A | 0.4726/0.4802 | N/A | N/A |
| DP-RT-RepAlt (laser alt.) | --- | --- | 0.4098/0.8942 | 1.6492/0.0129 | 0.3944/0.7332 |
| RP-RT-RepAlt (laser alt.) | --- | --- | --- | 1.2536/-0.0178 | 0.4096/0.745 |
| XO-RepAlt (radar alt.) | --- | --- | --- | --- | 0.4675/-0.229 |
| airborne | --- | --- | --- | --- | --- |

*Table 5: Summary of the ice cap SEC algorithm performance in relation to the selection criteria (Good=3 scores, Moderate=2 scores, Poor=1 score).*

| | **DS-RT-RepAlt** | **DP-RT-RepAlt** | **RP-RT-RepAlt** | **XO-RepAlt** |
|---|---|---|---|---|
| RMSE | Good | Good | Good | Poor |
| Spatial density | Good | Good | Good | Poor |
| Temporal density | Moderate | Moderate | Moderate | Good |
| Processing time | Good | Good | Good | Moderate |
| TOTAL SCORE | 11 | 11 | 11 | 7 |

## Figure captions

Fig. 1: Global map showing the location of the test regions described in this study.

Figure 2: Overlay of the glacier outlines from the different participants for the subset of test region GA4 where editing of wrong classification results was requested.

Figure 3: a) Three glacier maps combined resulting from three threshold values: 1.8 (all colours), 1.9: (grey and blue), 2.0 (grey). b) Effect of a 3 × 3 median filter: red pixels are removed and blue pixels are added (shown here for the map with the threshold 1.9).

Figure 4: Glacier outlines for the region shown in the inset with five different values of the threshold in band TM1 applied (blue: 100, green: 90, white: 80, red: 70, yellow: 60). Substantial changes take only place in regions with ice and snow located in cast shadow. The finally selected threshold in TM1 is 65.

- - - - - - -

Figure 5: (a) Hillshade of the SRTM DEM; (b) Elevation differences between the SRTM and 2006 ASTER DEM plotted in grayscale pre co-registration thus displaying the "false-hillshade"; (c) the elevation differences post co-registration; (d) histograms of the elevation differences pre- and post- co-registration; (e) plot of the slope normalized elevation differences by aspect pre co-registration and the solutions to equation XX after the first (blue) and second iterations (red); and (f) shows the same as e) but post co-registration.

- - - - - - -

Figure 6: scatter-plot of the dh/dt results obtained using the DP-RT-RepAlt and the RP-RT-RepAlt algorithms.

Figure 7: absolute differences in m/yr as function of the elevation between airborne dh/dt and DP-RT-RepAlt dh/dt (blu); airborne dh/dt and RP-RT-RepAlt dh/dt (purple); airborne dh/dt and XO-RepAlt dh/dt (green).

Figure 8: a) scatter-plot of the dh/dt results obtained using the DP-RT-RepAlt and the XO-RepAlt algorithms; b) scatter-plot of the dh/dt results obtained using the RP-RT-RepAlt and the XO-RepAlt algorithms.

- - - - - - -

Figure 9: From left to right: slant-range interferogram, slant-range and azimuth displacement maps from offset-tracking, and multiple-aperture interferogram based on a ALOS PALSAR image pair separated by 46 days over Vestfonna (Svalbard). Only offset-tracking is able to derive information over the outlet glaciers, the interferograms are decorrelated.

Figure 10: Results of the round robin with satellite optical data over Baltoro glacier. From top to bottom: NCC Dataset 1 unfiltered, NCC Dataset 1 filtered with correlation coefficient threshold and smoothing, NCC Dataset 2 unfiltered, NCC Dataset 3 weakly filtered, CCF-O filtered.

Figure 11: Displacement magnitude in slant range geometry over Breidamerkurjökull (Iceland) from various participant of the round-robin using the cross-correlation of chips in amplitude SAR images based on a TerraSAR-X image pair separated by 11 days. The following matching window sizes and oversampling factors were considered: Dataset 1: 128 x 128 / 2,

Dataset 2: 128 x 128 / 16, Dataset 3: 128 x 128 / 2, Dataset 4: 64 x 64 / 16, Dataset 5: 44 x 40 / 4 (to be checked).

Figure 12a: Polar plot of ground-range and azimuth displacements over stable ground (right) based on two results from the round-robin over Vestfonna (Svalbard) using a ALOS PALSAR image pair separated by 46 days. Standard deviations are on the order of 0.5 m, corresponding to total horizontal displacement rates of about 6 m/yr.

Figure 12b: Comparison of SAR and DGPS horizontal ice speeds over Vestfonna (Svalbard) using a ALOS PALSAR image pair separated by 46 days for two participants of the round-robin. DGPS data are from geodetic survey campaigns in 2007-2010 (Pohjola et al., 2011). The averages of the absolute difference between DPGS and SAR results are 9.6 m/yr and 7.6 m/yr in the two cases.

# Figures

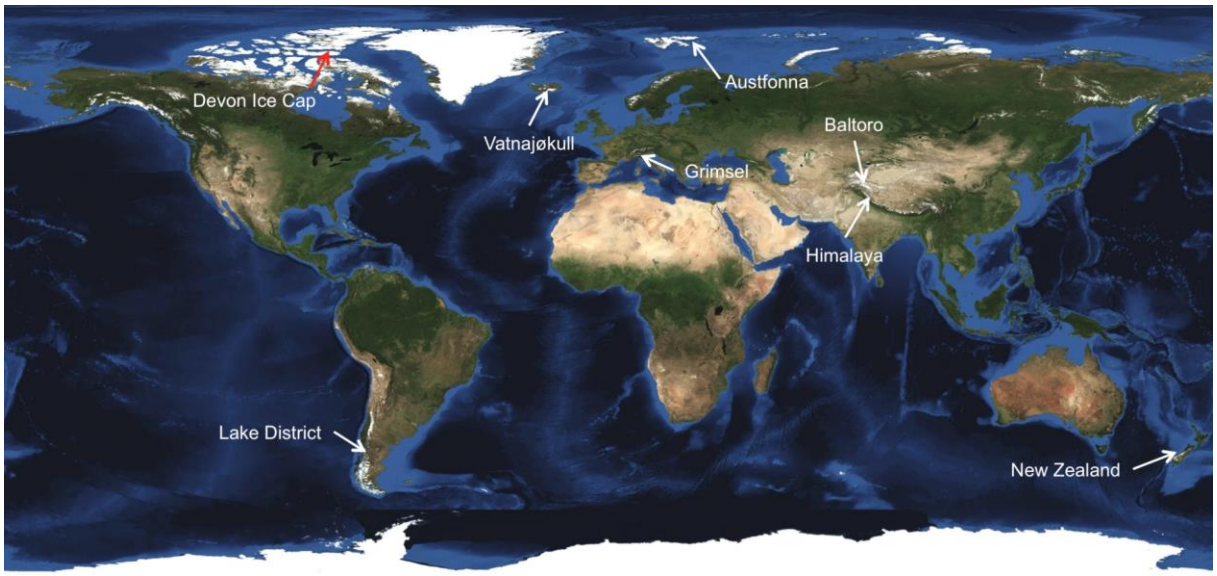


Fig. 1 Global overview map

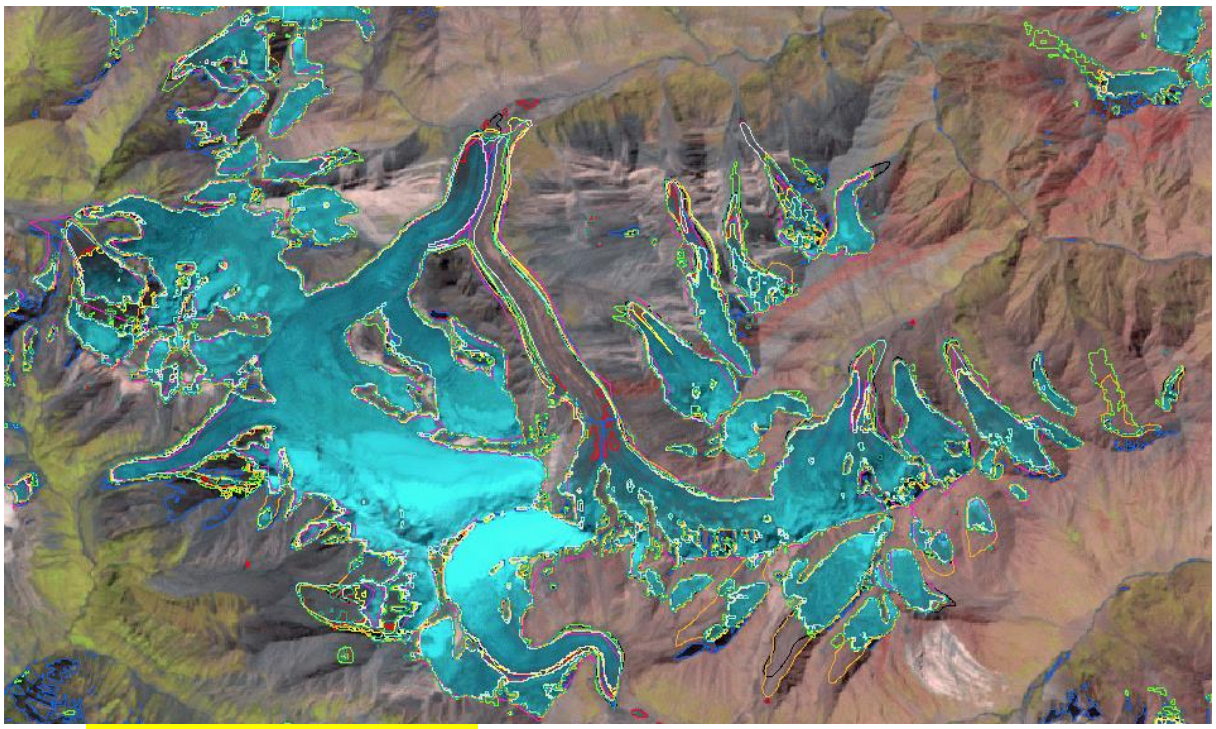

Fig. 2 XXX add scale bar and legend

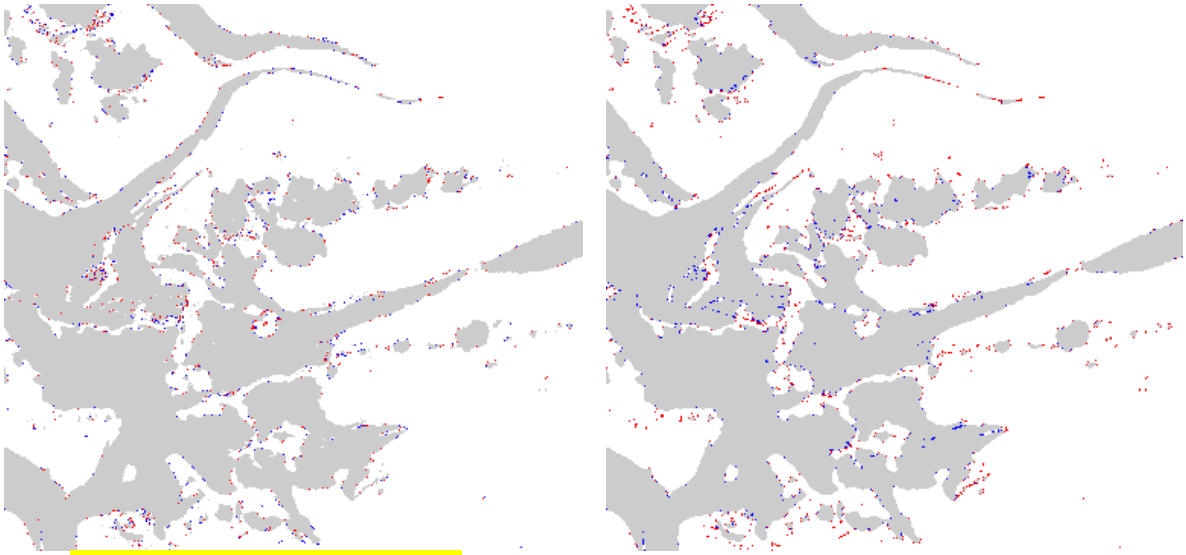

Fig. 3 XXX add scale bar and legend

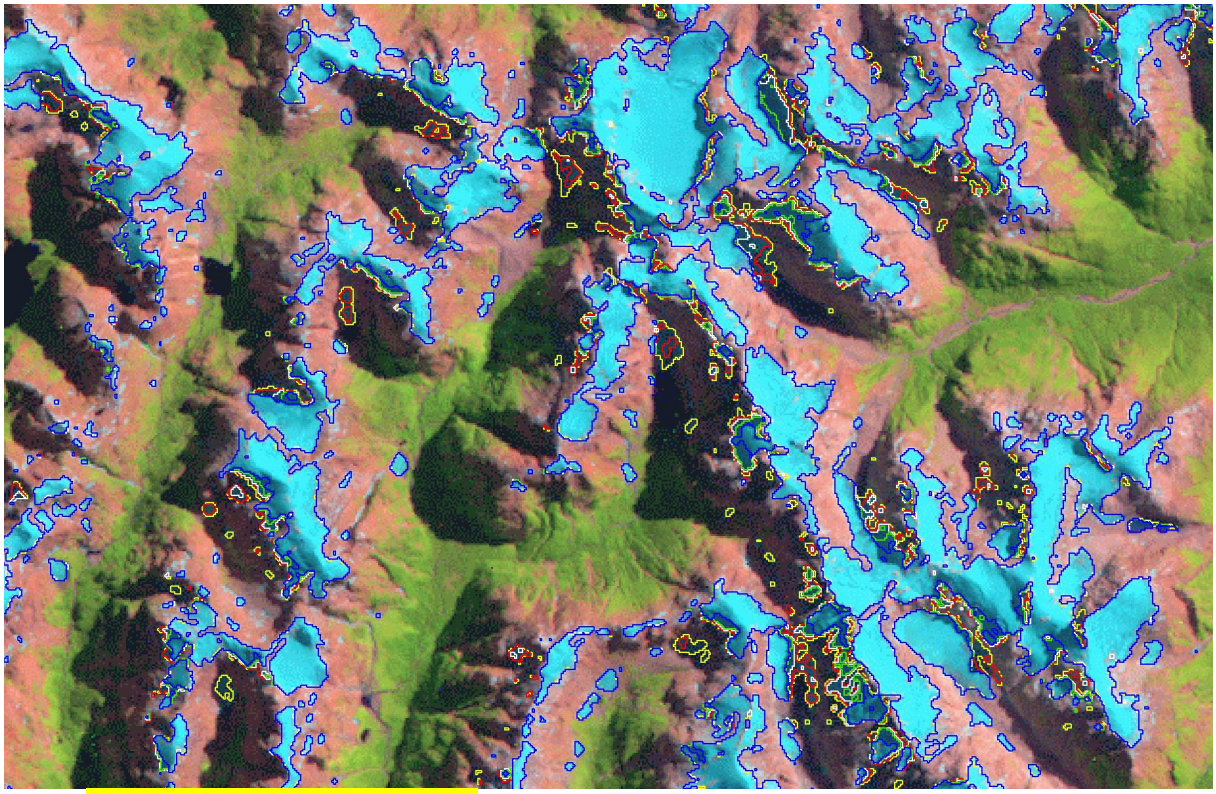

Fig. 4 XXX add scale bar and legend

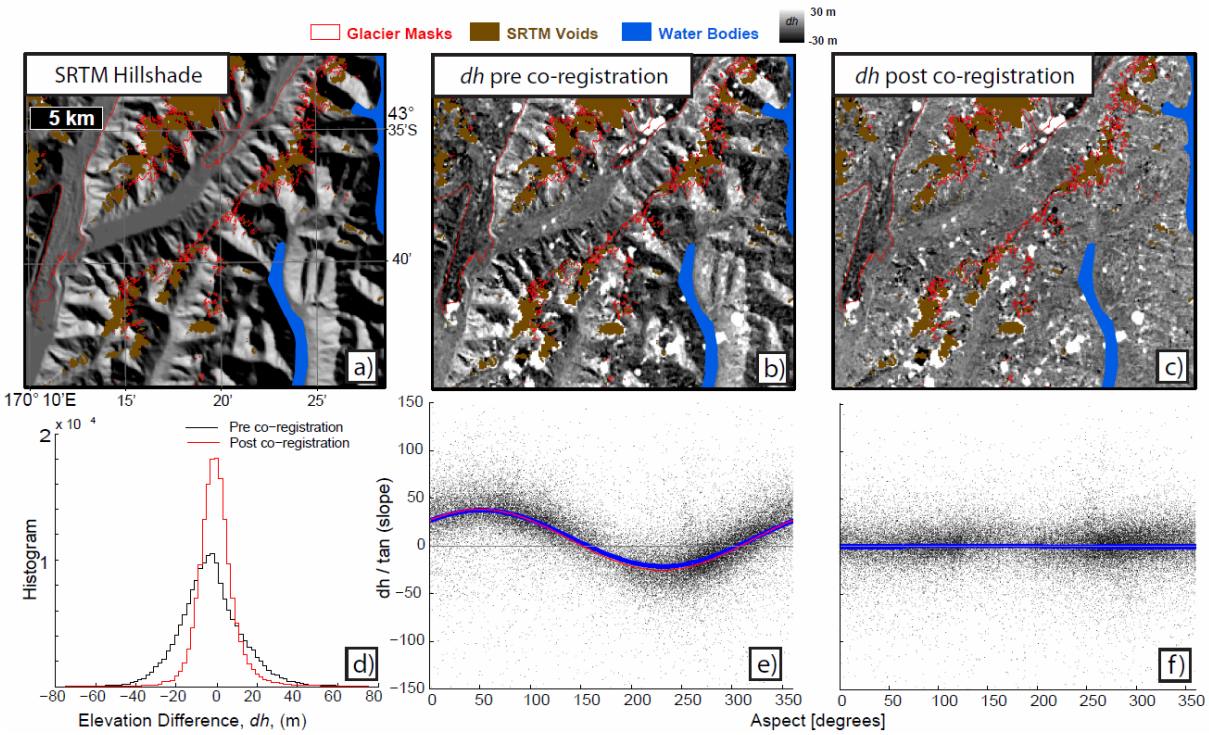


Fig. 5

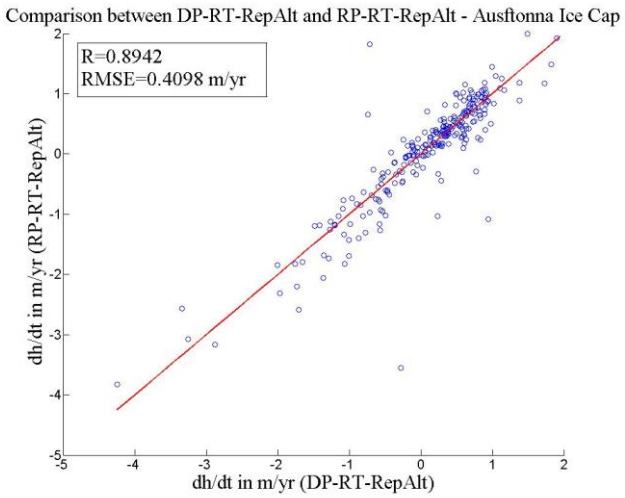


Fig. 6

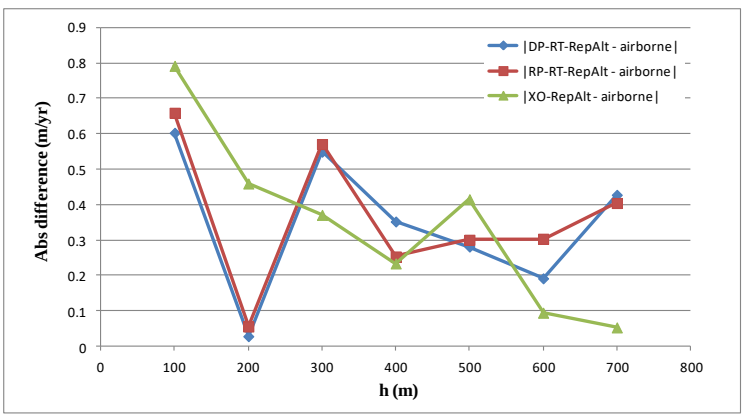


Fig. 7

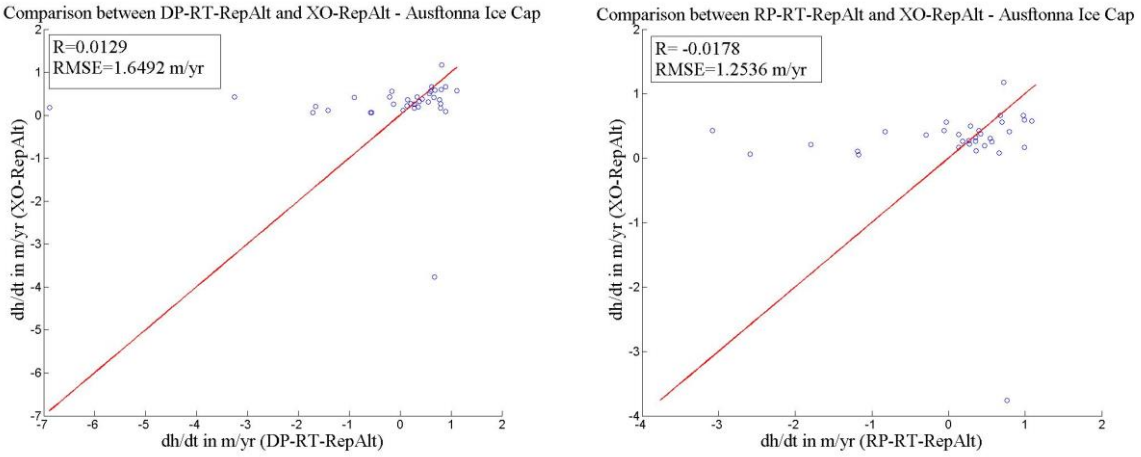


Fig. 8

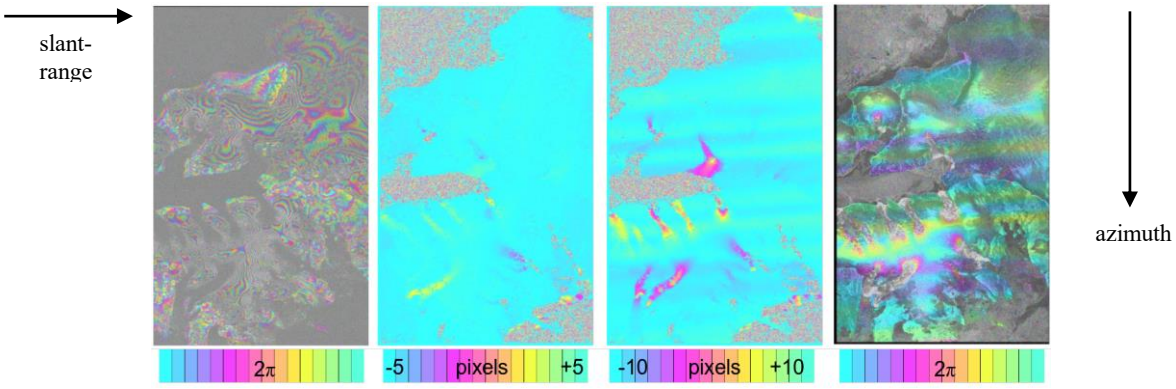


Fig. 9

*Fig 10 on next page*

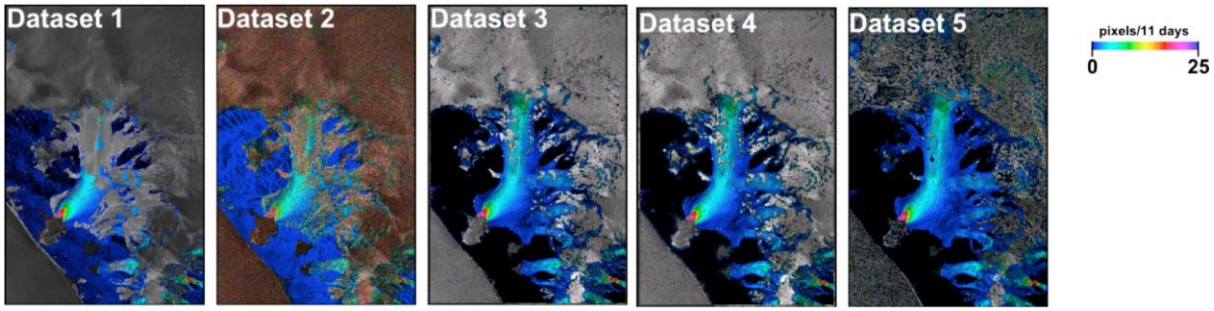


Fig. 11

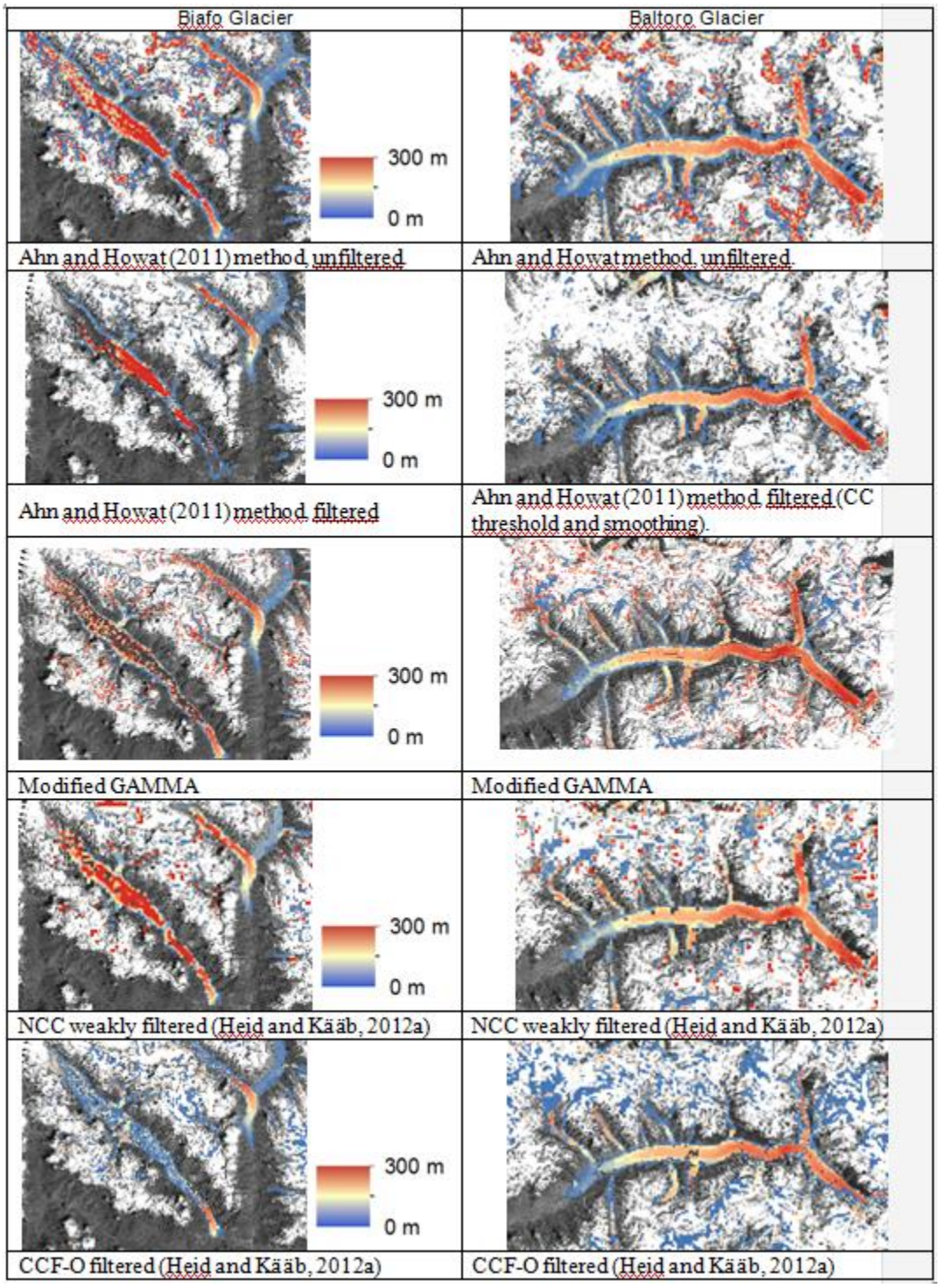
Biafo Glacier
Baltoro Glacier
300 m
0 m
Ahn and Howat (2011) method unfiltered
Ahn and Howat method unfiltered
Ahn and Howat (2011) method filtered
Ahn and Howat (2011) method filtered (CC threshold and smoothing).
Modified GAMMA
Modified GAMMA
NCC weakly filtered (Heid and Kääb, 2012a)
NCC weakly filtered (Heid and Kääb, 2012a)
CCF-O filtered (Heid and Kääb, 2012a)
CCF-O filtered (Heid and Kääb, 2012a)

Fig. 10

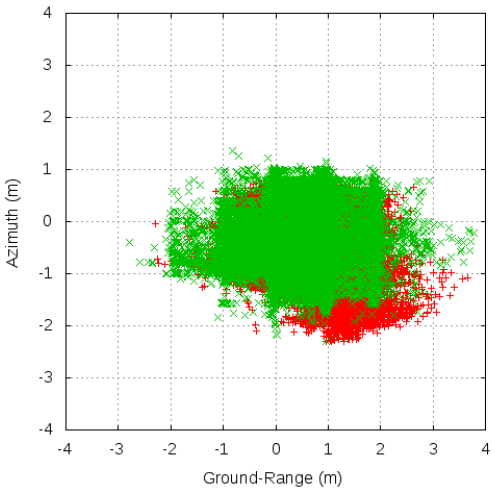


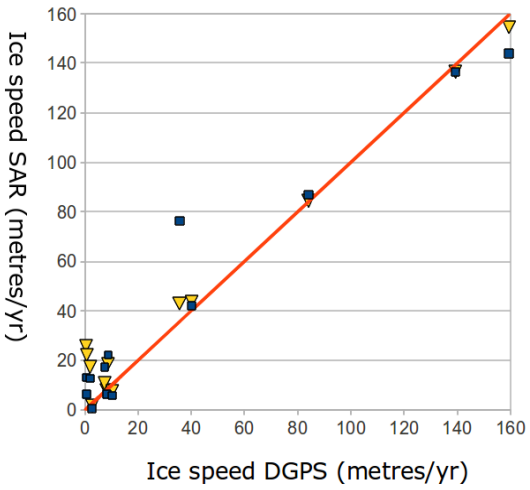


Fig. 12a and 12b

email list

Frank Paul[1], Tobias Bolch[1], Andreas Kääb[2], Thomas Nagler[3], Christopher Nuth[2], Killian Scharrer[3], Andrew Shepherd[4], Tazio Strozzi[5], Francesca Ticconi[4], Rakesh Bhambri[6], Etienne Berthier[7], Torborg Heid[2], Seongsu Jeong[8], Matthias Kunz[9], Adrian Luckman10, Alan Muir[11], Geir Moholdt[12], Jeffrey VanLooy[13], Thomas Van Niel[14]

tobias.bolch@geo.uzh.ch, andreas.kaab@geo.uio.no, thomas.nagler@enveo.at, christopher.nuth@geo.uio.no, kilian.scharrer@enveo.at, A.Shepherd@leeds.ac.uk, strozzi@gamma-rs.ch, F.Ticconi@leeds.ac.uk,

rakeshbhambri@gmail.com, etienne.berthier@legos.obs-mip.fr, torborg.heid@geo.uio.no, sjeong.kr@gmail.com, matthias.kunz@ncl.ac.uk, A.Luckman@swansea.ac.uk, asm@cpom.ucl.ac.uk, gmoholdt@ucsd.edu, jvanlooy@aero.und.edu, Tom.VanNiel@csiro.au

S.L.Bevan@swansea.ac.uk, mbraun@geographie.uni-erlangen.de, ngourmelen@unistra.fr, tomrune@norut.no, jme@space.dtu.dk, neelmeijer@gfz-potsdam.de

Suzanne Bevan, Swansea University, S.L.Bevan@swansea.ac.uk
Matthias Braun, University Erlangen, mbraun@geographie.uni-erlangen.de
Noel Gourmelen, University Strasbourg, ngourmelen@unistra.fr
Tom Rune Lauknes, NORUT, tomrune@norut.no
John Merryman, Danish Technical University (DTU), jme@space.dtu.dk
Julia Neelmeijer, GFZ Potsdam, neelmeijer@gfz-potsdam.de